https://doi.org/10.5194/egusphere-2023-438
Preprint. Discussion started: 28 March 2023

Impact of acidity and surface modulated acid dissociation on cloud response to organic aerosol

Gargi Sengupta[a], Minjie Zheng[a,b], and Nønne L. Prisle[a*]

[a]Center for Atmospheric Research, University of Oulu, P.O. Box 4500, 90014 Oulu, Finland
[b]Current affiliation: Institute for Atmospheric and Climate Science, ETH Zurich, Zürich, Switzerland

Correspondence: Nønne L. Prisle (Nonne.Prisle@oulu.fi)

Abstract.

Dissociation of organic acids is currently not included in most atmospheric aerosol models. Organic dissociation in aqueous aerosols could alter the H^+ concentrations and affect the cloud activating properties. We implemented a simple representation of organic dissociation in a box model version of the aerosol–chemistry–climate model ECHAM-HAMMOZ and investigated the impact on cloud droplet number concentrations and short-wave radiative effect through changes in kinetically driven sulfate concentrations in an aerosol population. Organic dissociation has been observed in X-ray photo-electron spectroscopy measurements to be significantly suppressed in the aqueous surface. We therefore additionally introduced an empirical account of this mechanism to explore the potential further impact on aerosol effects. Malonic acid and decanoic acid were used as proxies for atmospheric organic acid aerosols. Both acids were found to yield sufficient hydrogen ion concentrations from dissociation in an aqueous droplet population to strongly influence the sulfur chemistry, leading to enhanced cloud droplet number concentrations and a cooling short-wave radiative effect. Further considering surface modulated suppressed dissociation, the impact on cloud microphysics was smaller than according to the well-known bulk solution organic dissociation, but still significant. Our results show that organic aerosol acidity can significantly influence predictions of aerosol formation and aerosol-cloud-climate effects. Furthermore, it may be important to also consider the specific influence of surface effects, also in relation to bulk solution phenomena such as organic acid dissociation.

1 Introduction

Atmospheric aerosols are an important contributor to Earth's climate. They may either absorb or reflect heat and sunlight, directly affecting Earth's energy budget (IPCC et al., 2007). Aerosols also contribute to the global climate through indirect effects where they serve as the necessary seeds for cloud formation. The chemical composition of aerosols is complex and includes numerous organic and inorganic species (O'Dowd et al., 2004; Putaud et al., 2010; Murphy et al., 2006). Organic compounds have been reported to comprise approximately 20 to 50% of the total aerosol mass at mid-latitude regions (Saxena and Hildemann, 1996; Putaud et al., 2004) and much higher (approximately 90%) in tropical forests (Andreae and Crutzen, 1997; Roberts et al., 2001; Kanakidou et al., 2005). Significant amounts of organic aerosols (approximately 70%) are also reported in the middle troposphere (Huebert et al., 2004). Despite their abundance and importance, the organic fraction is the

https://doi.org/10.5194/egusphere-2023-438
Preprint. Discussion started: 28 March 2023

least understood component of atmospheric aerosols and the uncertainty around organic aerosols and their interaction with clouds remains one of the largest overall sources of uncertainty in climate projections (IPCC, 2013; Seinfeld et al., 2016; Legg, 2021). This is due, in part, to a limited representation of organic aerosol (OA) processes and properties in climate models, such as organic acidity and surface activity of the organic components (Kanakidou et al., 2005; Prisle et al., 2012a; Freedman et al., 2018; Pye et al., 2020).

The acidity of aqueous aerosol droplets, reported in terms of pH, is one of its most fundamental chemical properties, driving key chemical reactions that ultimately impact global climate in numerous ways (Ault, 2020). The aerosol acidity representation in climate models uses observationally-based proxies, which serve as a universal pH indicator in simulations, however, these proxies do not represent the entire aerosol population accurately (Pye et al., 2020). Studies comparing different model estimates of pH using the same inputs differ on average by 0.3 pH units (but can vary up to 1 pH unit, increasing with decreasing relative humidity) depending on the model framework used and the approach for estimating the H^+ activity coefficient (Peng et al., 2019; Ruan et al., 2022; Battaglia Jr et al., 2021). While gas-particle partitioning and ionic equilibria are the dominant factors that drive aerosol acidity, models are frequently lacking H^+ that is kinetically generated as a result of transient gas- and liquid-phase chemical reactions (Li et al., 2022; Tilgner et al., 2013). Additionally, the organic fraction, which often comprises significant amounts of components with acid functionality, is considered as un-dissociated and the H^+ concentration in aerosols is assumed to have no contribution from the organic fraction (Kanakidou et al., 2005; Hennigan et al., 2015). The dissociation of the organic fraction in aqueous aerosols could play a significant role in the measure of aerosol acidity and influence chemical processes within the aerosol, such as the oxidation of sulfur dioxide by H_2O_2 and O_3, leading to increased sulfate concentrations in the aqueous aerosols (Liu et al., 2020). The inclusion of organic dissociation in climate models could impact fundamental aerosol chemical processes and therefore, have a significant impact on the cloud activation properties of aqueous aerosols.

Surface active organics (surfactants) have been reported in atmospheric aerosols from many different regions and environments (Gérard et al., 2016; Petters and Petters, 2016; Nozière et al., 2017; Kroflič et al., 2018; Gérard et al., 2019). In liquid mixtures, such as aqueous solution droplets, surfactants can adsorb at the interfaces, lowering the surface tension and inducing concentration gradients between the droplet surface and bulk solution (Prisle et al., 2010; Bzdek et al., 2020; Lin et al., 2018; Malila and Prisle, 2018; Lin et al., 2020; Prisle, 2021). The bulk-surface partitioning may be significant in small droplets like atmospheric aerosols due to the high surface area to bulk volume ratio. Therefore, surface properties should be explicitly considered to represent surface active aerosols in climate models (Prisle et al., 2010, 2012a).

Synchrotron-radiation-based X-ray photoelectron spectroscopy (XPS) measurements in the surface region of aqueous solutions containing surface-active carboxylate ions have been used to study the acid-base speciation at the surface (Prisle et al., 2012b; Öhrwall et al., 2015; Werner et al., 2018). These studies revealed that the protonated form of the surfactant carboxylates was found at an extraordinarily large fraction compared to that expected from the bulk pH. Specifically, (Werner et al., 2018) found that the surface acid-base equilibrium of mono-carboxylic acids was shifted by 1 – 2 pH units compared to the bulk acidity across a wide range of bulk pH. Very few studies have investigated the consequences of varying organic acidity on cloud activation (Tilgner et al., 2021a; Angle et al., 2021; Li et al., 2020; Franco et al., 2021) and to the best of our knowledge,

https://doi.org/10.5194/egusphere-2023-438
Preprint. Discussion started: 28 March 2023

organic dissociation accounting for surface specific effects in aqueous aerosols has never been implemented and studied in a cloud activation model.

In this work, we introduce organic dissociation in the aerosol–chemistry-climate box model ECHAM6.3–HAM2.3 (Kokkola et al., 2018; Tegen et al., 2019), and assess its impact on sulfur chemistry and cloud activation process via cloud droplet number concentrations (CDNC) and short-wave radiative effect (RE), as examples of key processes taking place in organic aqueous aerosols and droplets. We also implement a simple representation of surface modulated suppressed organic dissociation and investigate the significance of such an effect for predictions of aerosol–cloud–climate effects.

2 Methods

We first introduce an account of organic dissociation and then augment it with a simple representation to further account for the surface-driven suppression of dissociation observed in XPS measurements. The impact of organic aerosol acidity and surface-driven suppressed dissociation on the sulfur chemistry and cloud microphysics is then assessed. We use ECHAM6.3–HAM2.3 (referred to here as HAMBOX), which is a box model version of the aerosol–chemistry–climate model ECHAM–HAMMOZ (Tegen et al., 2019). HAMBOX includes the SALSA2.0 sectional aerosol module as described by Kokkola et al. (2018). We calculate the cloud droplet number concentrations (CDNC) for an air parcel, based on the predicted total aerosol population sulfate mass accounting for the surface specific effects, and compare to predictions for identical conditions without accounting for organic dissociation. The resulting CDNC is then used to estimate the short-wave radiative effect (RE) from cloud formation using the method of Bzdek et al. (2020).

2.1 Aerosol module in HAMBOX

HAMBOX uses the SALSA2.0 aerosol module (Kokkola et al., 2018). In SALSA2.0, the aerosol size distribution is calculated using the sectional approach (Jacobson, 2005) and represented using 10 size bins i. Here, we group the 10 size bins into four sub-ranges: Nucleation (i = 1 and 2) with mean particle diameter, $\bar{d}_p$ = 56 nm; Aitken (i = 3, 4 and 5) with $\bar{d}_p$ = 160 nm; Accumulation (i = 6, 7 and 8) with $\bar{d}_p$ = 485 nm and Coarse (i = 9 and 10) with $\bar{d}_p$ = 1.85 µm. The initial number concentration in each sub-range (shown in Table 1) used for all HAMBOX simulations is reflective of a moderately polluted environment (von Bismarck-Osten et al., 2013). As a property of the sectional approach, when particles grow or shrink out of the boundaries of their size bins, they are redistributed to new size bins and the new aerosol size distribution is calculated at each time step.

https://doi.org/10.5194/egusphere-2023-438
Preprint. Discussion started: 28 March 2023

Table 1. Initial aerosol number concentration in each size sub-range used in HAMBOX SALSA2.0 model.

Sub-range	Number concentration [N/cm^3]	Geometric mean diameter [µm] & Standard deviation
Nucleation	100	0.01 & 1.50
Aitken	400	0.3 & 1.50
Accumulation	200	1.0 & 1.50
Coarse	0	3.0 & 2.0

A sulfur chemistry module (Feichter et al., 1996a) is coupled to the growth module in SALSA2.0 through time step. The sulfur chemistry module feeds in the calculated sulfate mass fraction in the aerosol population to the growth module, the growth module undergoes an aerosol redistribution and feeds back the new aerosol size distribution and chemical composition to the sulfur chemistry module, in each time step. The chemical compounds in SALSA2.0 are represented by model compound classes: 'sulphate' (SU), 'organic carbon' (OC), 'sea salt' (SS), 'black carbon' (BC) and 'mineral dust' (DU). We consider five different initial conditions with different organic mass fractions, denoted by $\chi_{\mathrm{OA}} = \{0.2, 1\}$, to represent different environments where OA have been reported in varying concentrations. For example, in boreal forest environments, OA mass fraction is reported around 0.6 (Äijälä et al., 2019), and in marine environments, around 0.2 (O'Dowd et al., 2004). χ_{OA} = 1 is a hypothetical extreme where we consider thhe entire aerosol to contain only organic carbon. The initial mass fractions of all model compounds in these five conditions are shown in Table 2. Here, the sulfur chemistry module is used to calculate the total sulfate mass in the aerosol population based on varying hydrogen ion concentration in the aqueous aerosol, considering no organic dissociation, bulk organic dissociation and surface modulated organic dissociation. Following this, we use HAMBOX cloud microphysics to calculate CDNC and consequent short-wave radiative effect (RE) for each of these imposed conditions.

Table 2. Initial mass fractions of all model compounds in the five different $\chi_{\mathrm{OA}} = \{0.2, 1\}$ considered.

χ_{OA}	Sulfate (SU)	Organic (OC)	Black carbon (BC)	Sea salt (SS)	Mineral dust (DU)
0.2	0.4	0.2	0.05	0.1	0.25
0.4	0.4	0.4	0.05	0.05	0.1
0.6	0.4	0.6	0	0	0
0.8	0.2	0.8	0	0	0
1	0	1	0	0	0

2.2 Cloud microphysics in HAMBOX

The HAMBOX cloud microphysics used in this work includes the calculation of critical supersaturation (S_i) and the activated fraction (n_i) for each bin i. A detailed description of the parameterizations and equations used to derive these cloud activation factors are available in Abdul-Razzak (2002) and Abdul-Razzak et al. (1998).

https://doi.org/10.5194/egusphere-2023-438
Preprint. Discussion started: 28 March 2023

First, the maximum critical supersaturation ($S_{\max}$) for the air parcel is calculated by

$$S_{\max} = \frac{S_e}{\left[0.5\left(\frac{\varsigma}{\eta}\right)^{3/2} + \left(\frac{S_e^2}{\eta+3\zeta}\right)^{3/4}\right]^{1/2}}, \tag{1}$$

where η is the surface tension correction factor and ζ is the correction factor for Kelvin term in the Köhler curve (for details, see Eqs 5 and 6 in Abdul-Razzak and Ghan (2002)). S_e is the effective critical supersaturation for the air parcel,

$$S_e^{2/3} = \frac{\sum_{i=1}^{I} N_i}{\sum_{i=1}^{I} N_i / S_i^{2/3}}. \tag{2}$$

Here i is the number of bins, S_i is the critical supersaturation for each bin, and N_i is the number of particles in each bin. S_i is given by

$$S_i = \exp\left(\frac{A}{D_{\text{wet}}} - \frac{B}{D_{\text{wet}}^3 - d_p^3}\right) - 1, \tag{3}$$

where D_{wet} and d_p are droplet diameter and dry particle diameter, respectively. The terms A and B are calculated as

$$A = \frac{4M_w\sigma_w}{RT\rho_w}, \quad B = \frac{6n_sM_w}{\pi\rho_w}, \tag{4}$$

where M_w is the molecular weight of water = 0.018 kgmol^{-1}, σ_w is the surface tension of pure water = 0.073 Nm^{-1} , ρ_w = 1000 kgm^{-3} is the density of water, R = 8.314 $\text{JK}^{-1}\text{mol}^{-1}$, temperature T = 293 K and n_s is the number of moles of solute obtained from χ_{OA}.

Once the maximum supersaturation of the air parcel is determined, the activation of each bin is determined by comparing $S_{\max}$ with S_{il} and S_{iu} (the lower and upper critical supersaturation bounds of the bin). The number of activated particles (n_i) in each size bin (i) is given by

$$n_i = 0, \quad \text{if} \quad S_{\max} < S_{il}, \tag{5}$$

$$n_i = \frac{\log(S_{\max}/S_{il})}{\log(S_{iu}/S_{il})}, \quad \text{if} \quad S_{il} \le S_{\max} \le S_{iu}, \tag{6}$$

and

$$n_i = 1, \quad \text{if} \quad S_{iu} < S_{\max}. \tag{7}$$

S_{il} and S_{iu} are obtained using equation 3 for the diameters of the smallest particle (d_{il}) and biggest particle (d_{iu}) in each size bin. The average activated fraction for all size bins (n) is then calculated by

$$n = \frac{\sum n_i}{\sum N_i}. \tag{8}$$

https://doi.org/10.5194/egusphere-2023-438
Preprint. Discussion started: 28 March 2023

The total number of activating particles is given by the cloud droplet number concentration (CDNC), which is calculated using the number of activating particles within each size bin,

$$\mathrm{CDNC} = \sum_{i=1}^{I} N_i n_i. \tag{9}$$

The CDNC calculated using equation 9 accounting for organic acid dissociation is denoted by $\mathrm{CDNC_{HA}}$ and the change in CDNC (ΔCDNC) with respect to no organic dissociation ($\mathrm{CDNC_0}$) is

$$\Delta\mathrm{CDNC} = \frac{\mathrm{CDNC_{HA}} - \mathrm{CDNC_0}}{\mathrm{CDNC_0}} \tag{10}$$

We estimate the change in short-wave radiative effect (RE) from the change in sulfate mass as a consequence of surface modulated organic acidity. The change in cloud-top albedo (Δa) at constant cloud liquid water content (LWC = 0.03 $\mathrm{gm^{-3}}$, Thompson (2007)) is calculated from the change in CDNC (ΔCDNC) following Bzdek et al. (2020)

$$\Delta a = \mathrm{LWC}(1 - \mathrm{LWC})\Delta\mathrm{CDNC}/(3\mathrm{CDNC}). \tag{11}$$

The short-wave radiative effect (RE) is then calculated as

$$\mathrm{RE} \approx -F_0 E_{\mathrm{LWC}} T_{\mathrm{LWC}}^2 \Delta a, \tag{12}$$

where $F_0 = 340\ \mathrm{Wm^{-2}}$ is the incoming solar flux at the top of the atmosphere. In Equation 12, $E_{\mathrm{LWC}} = 0.3$ is the fractional coverage of different types of clouds, and $T_{\mathrm{LWC}} = 0.76$ is the transmittance of the atmosphere at visible wavelengths, constant for all simulations. For the default HAMBOX cloud microphysics calculations, cloud temperature is taken as 271 K, cloud pressure is 101 kPa, cloud fraction is 0.3, saturation ratio of gas phase water is 0.3, and updraft velocity is 0.3 $\mathrm{ms^{-1}}$. The simulation time for all calculations was taken as 1 hour with 1 second time steps.

2.3 Sulfur chemistry in HAMBOX

We use the aqueous sulfur chemistry module of Feichter et al. (1996b) (with modifications described below) to calculate the total sulfate concentration ($[\mathrm{SO_4^{2-}}]$) in the aerosol population from the oxidation of $\mathrm{SO_2}$ by $\mathrm{H_2O_2}$ and $\mathrm{O_3}$ in the aqueous droplets. The reaction rate for the $\mathrm{H_2O_2}$ oxidation pathway can be written as:

$$\frac{\partial}{\partial t}\left[\mathrm{SO_4^{2-}}\right] = \frac{k_4\left[\mathrm{H_2O_2}\right]\left[\mathrm{SO_2}\right]}{\left[\mathrm{H^+}\right] + 0.1} \tag{13}$$

where the rate constant k_4 is calculated by

$$k_4 = 8 \times 10^4 \exp\left(-3650\left(\frac{1}{T} - \frac{1}{298}\right)\right), \tag{14}$$

where T is the cloud temperature = 271 K. Equation 13 is known to be pH- insensitive (Liu et al., 2020) and is used in this work to determine the total sulfate concentration from the $\mathrm{H_2O_2}$ oxidation for simulations where organic dissociation is not considered.

https://doi.org/10.5194/egusphere-2023-438
Preprint. Discussion started: 28 March 2023

To calculate the total sulfate concentration from the H_2O_2 oxidation pathway accounting for pH dependency arising from organic dissociation and further surface modulated organic acidity, we follow the procedure given by Liu et al. (2020), which is valid for pH >2. Here we use the general acid catalysis reaction mechanism where SO_2 in an aqueous environment exists as the HSO_3^- anion and reacts with H_2O_2 in the presence of an organic acid (HA) catalyst, which acts as a proton donor (Maaß et al., 1999; McArdle and Hoffmann, 1983). Briefly, the overall reaction mechanism may be represented as

$$HSO_3^- + H_2O_2 \rightleftharpoons HOOSO_2^- + H_2O \tag{R1}$$

$$HOOSO_2^- + HA \rightarrow 2H^+ + SO_4^{2-} + X^- \tag{R2}$$

The rate expression for R1-R2 is

$$\frac{\partial}{\partial t}\left[SO_4^{2-}\right] = \left(k + \frac{k_{HA}[HA]}{[H^+]}\right) K_{a1}[SO_2][H_2O_2], \tag{15}$$

where K_{a1} is the thermodynamic dissociation constant of H_2SO_3 and k is a constant derived from the reaction rate coefficient and the thermodynamic equilibrium constants. k_{HA} is the overall rate constant for the general acid catalysis mechanism approximated by $\log k_{HA} = -0.57(pK_a) + 6.83$ (Liu et al., 2020; Drexler et al., 1991).

The total sulfate concentration from O_3 oxidation is given by

$$\frac{\partial}{\partial t}\left[SO_4^{2-}\right] = \left(k_{51} + \frac{k_{52}}{[H^+]}\right)[O_3]\,[SO_2]\,, \tag{16}$$

where rate constants k_{51} and k_{52} are calculated by:

$$k_{51} = 4.39 \times 10^{11} \exp\left(\frac{-4131}{T}\right) \tag{17}$$

$$k_{52} = 2.56 \times 10^{3} \exp\left(\frac{-996}{T}\right). \tag{18}$$

Sulfate concentrations thus calculated in the aqueous phase chemistry module is distributed to pre-existing size bins in SALSA2.0.

The $[H^+]$ concentrations in the sulfur chemistry module are obtained from water and aqueous phase sulfate concentrations. Here, the default HAMBOX $[H^+]$ is denoted by $[H^+]_0$ and gives the $[H^+]$ concentrations when no organic dissociation (no diss) is considered.

$$\left[H^+\right]_0 = \left[H^+\right]_{\text{initial}} + \frac{\left[SO_4^{2-}\right]}{\text{LWC} \times \text{MW}_{SO_4^{2-}}}, \tag{19}$$

where LWC is the liquid water content in cloud ($\mathrm{g m^{-3}}$), $[SO_4^{2-}]$ is the summation of soluble sulfate in all bins. $\text{MW}_{SO_4^{2-}}$ is the molar weight of the sulfate anion ($\mathrm{g\,mol^{-1}}$). $[H^+]_{\text{initial}}$ is the hydrogen ion concentration obtained from the cloud pH

https://doi.org/10.5194/egusphere-2023-438
Preprint. Discussion started: 28 March 2023

(uniform for all bins) set to pH=5, giving initial hydrogen ion concentration ($[H^+]_{initial}$, eq.19) of 2.5×10^{-6} molesl^{-1}. For all simulations in the sulfur chemistry module, we assume $[SO_2]$, $[H_2O_2]$ and $[O_3]$ in cloud are fixed at 5 ppb, 1 ppb and 50 ppb, respectively (Tilgner et al. (2021b)). We introduce organic dissociation and modify equation (19) to get the total hydrogen ion concentration in the aerosol population,

$$\left[H^+\right]_{tot} = \left[H^+\right]_{initial} + \frac{\left[SO_4^{2-}\right]}{LWC \times MW_{SO_4^{2-}}} + \left[H^+\right]_{HA}, \tag{20}$$

where $[H^+]_{HA}$ is the concentration of the hydrogen ions dissociated by the OA.

The relative change in hydrogen ion concentration ($\Delta[H^+]$), with respect to 'no diss' is given by

$$\Delta\left[H^+\right] = \frac{[H^+]_{tot} - [H^+]_0}{[H^+]_0} \times 100, \tag{21}$$

and the corresponding relative change in sulfate concentration compared to 'no diss' is

$$\Delta\left[SO_4^{2-}\right] = \frac{\left[SO_4^{2-}\right] - \left[SO_4^{2-}\right]_0}{\left[SO_4^{2-}\right]_0} \times 100, \tag{22}$$

where $\left[SO_4^{2-}\right]$ is the sulfate concentration considering organic dissociation and $\left[SO_4^{2-}\right]_0$ is the sulfate concentration for 'no diss'.

The $[H^+]_{tot}$ thus calculated is used to obtain the total sulfate concentration in the aerosol population from H_2O_2 oxidation using eq. 15 and from O_3 oxidation using eq. 16, for varying conditions of organic dissociation (different $[H^+]_{HA}$ from bulk and surface apparent pK_a). The sulfate concentrations thus obtained gives a modified sulfate mass fraction (SU in section 2.1 and table 2) in the entire aerosol population.

2.4 Organic Dissociation

The dissociation behavior of monoprotic and diprotic acids, under similar dissociation environments, differ greatly from each other and different kinetic equations are used to describe them. We consider both treatments of organic dissociation to show two examples of dissociation behavior.

2.4.1 Dissociation of monoprotic acids

The dissociation of a monoprotic organic acid (HA) in an aqueous medium may be represented by the equilibrium

$$HA + H_2O \rightleftharpoons A^- + H_3O^+ \tag{R3}$$

where H^+ from the dissociation of the organic acid are considered as fully hydrated, such that the concentration of H_3O^+ is equivalent to the concentration of hydrogen ions from dissociation of HA.

The equilibrium acid dissociation constant is

$$K_a = \frac{a_{H_3O^+} a_{A^-}}{a_{HA}}, \tag{23}$$

https://doi.org/10.5194/egusphere-2023-438
Preprint. Discussion started: 28 March 2023

where $a_{H_3O^+}, a_{A^-}$ and a_{HA} are the activities of H_3O^+cations, A^-anions and HA molecules, respectively. Eq. 23, can be approximated in terms of the molar concentrations and ideal-dilute molar concentration based activity coefficients (γ_i) of each species i as:

$$K_a = \frac{[H_3O^+][A^-]}{[HA]} \frac{\gamma_{H_3O^+}\gamma_{A^-}}{\gamma_{HA}}. \quad (24)$$

Since HA is a monoprotic acid with only one ionsizable hydrogen,

$$[A^-] = [H_3O^+], [HA] = [HA]_{tot} - [H_3O^+], \quad (25)$$

where $[HA]_{tot}$ is the total concentration of the organic acid. The acid dissociation degree α is defined as

$$\alpha = \frac{[A^-]}{[HA]_{tot}} = \frac{[H_3O^+]}{[HA]_{tot}}. \quad (26)$$

Combining equations (24) and (26) and approximating $\frac{\gamma_{H_3O^+}\gamma_{F^-}}{\gamma_{HF}}$ with the mean activity coefficient $\gamma_\pm$,

$$K_a = [HA]_{tot} \frac{\alpha^2}{1-\alpha} \gamma_\pm^2 \quad (27)$$

For a highly diluted solution (e.g., $[HA]_{tot}$ <0.001 $moll^{-1}$), $\gamma_\pm^2$ can be assumed as 1. Under these conditions, equation (27) can be written as

$$\alpha = \frac{-K_a + \sqrt{K_a^2 + 4K_a \times [HA]_{tot}}}{2[HA]_{tot}} \quad (28)$$

2.4.2 Dissociation of diprotic acids

For a diprotic organic acid (H_2A), the dissociation of H^+ ions in an aqueous medium occurs in two stages:

$$H_2A + H_2O \rightleftharpoons HA^- + H_3O^+ \quad (R4)$$

and

$$HA^- + H_2O \rightleftharpoons A^{2-} + H_3O^+. \quad (R5)$$

The dissociation constant for R4 is the first dissociation constant of the diprotic acid denoted as K_{a1} and the dissociation constant for R5 is the second dissociation constant of the diprotic acid, denoted as K_{a2}. The overall dissociation constant of the diprotic acid is

$$\beta = K_{a1}K_{a2}, \quad (29)$$

and therefore,

$$p\beta = pK_{a1} + pK_{a2}. \quad (30)$$

https://doi.org/10.5194/egusphere-2023-438
Preprint. Discussion started: 28 March 2023

Using similar assumptions as the monoprotic acid, for a highly dilute solution, the acid dissociation degree α for a diprotic acid can be derived as:

$$\alpha = \frac{1}{4\beta[\mathrm{H_2A}]_{\mathrm{tot}} + 2}, \tag{31}$$

where, $[\mathrm{H_2A}]_{\mathrm{tot}}$ is the total concentration of the diprotic acid. Thus, based on the known pK_a and organic concentrations $[\mathrm{HA}]_{\mathrm{tot}}$ and $[\mathrm{H_2A}]_{\mathrm{tot}}$ derived from the OA mass fraction, we calculate the dissociation degree (α) of the organic acids, following which the amount of $\mathrm{H^+}$ ions dissociated by the organic acid is calculated for the bulk solution.

2.4.3 van't Hoff factor for organic dissociation

The dissociation of the solutes influences the available moles of solute in aerosol particles, affecting the water activity and critical supersaturation calculations in the model. The van't Hoff factor for organic dissociation (i_{OA}) is related to the dissociation degree, α (shown in eq. 28 and 31) as

$$i_{\mathrm{OA}} = 1 + \alpha(n_{\mathrm{ions}} - 1), \tag{32}$$

where n_{ions} is the number of ions formed from one formula unit of the organic acid.

The available moles of the solute n_s in SALSA2.0 is calculated as

$$n_s = i_{\mathrm{SU}} n_{\mathrm{SU}} + i_{\mathrm{OA}} n_{\mathrm{OA}} + i_{\mathrm{SS}} n_{\mathrm{SS}}, \tag{33}$$

where the n_{SU}, n_{OA} and n_{SS} are the initial number of moles of sulfate, organic aerosol and sea salt, respectively, while i_{SU}, i_{OA} and i_{SS} are the corresponding van't Hoff factors. The available molar amount of the solute n_s influences the critical supersaturation of the bins (the Raoult term B in eq. 3) and maximum critical supersaturation S_{max}, thereby affecting the critical supersaturation for each bin (S_i) and consequently the activation processes. In SALSA2.0, the sulfate and sea salt are considered as fully dissociated and i_{SU} and i_{SS} are set to 3 and 2, respectively. By default, organic aerosol is not considered as dissociated and i_{OA} is set equal to 1. Here, we assume that the entire organic aerosol is an organic acid and the i_{OA} is calculated using eq. 32, for the surface and bulk representation of organic dissociation. The total available moles of solute (n_s, eq. 33) is thus modified for organic dissociation and is then reflected in the Raoult term, B (eq. 4) which changes the critical supersaturation S_i for each bin. The change in Raoult term and S_i from inclusion of organic dissociation in van't Hoff factor, i_{OA}, is independent of the kinetic $[\mathrm{H^+}]$ driven sulfate concentrations in the aqueous aerosol, and is instead a measure of the change in water activity due to the dissociation of the organic acid and the consequent increase in the number of available moles of solute, n_s.

2.4.4 Representation of bulk and surface modulated organic dissociation

We assume the entire OA to be an organic acid and consider it to be dissociated according to α calculated using reported pK_a values from literature, using eqs. 28 and 31 for monoprotic and diprotic acids, respectively. This representation of organic dissociation does not account for any surface specific effects and represents organic dissociation in the aqueous aerosol bulk,

https://doi.org/10.5194/egusphere-2023-438
Preprint. Discussion started: 28 March 2023

and is denoted as pK_a^{bulk}. For the monoprotic acid pK_a^{bulk} is the reported first pK_a readily available from literature, whereas for the diprotic acid, the sum of the reported first and second pK_a, available in literature, is taken as pK_a^{bulk} (same as $p\beta$, eq. 30).

Previous work has shown that for aerosol particles comprising surface active organic acids and their salts, such as sodium octanoate, sodium decanoate, sodium dodecanoate, and sodium dodecyl sulfate, during major part of hygroscopic growth and cloud droplet activation, almost all surface active OA is partitioned to the surface (Prisle et al., 2010, 2011; Lin et al., 2018, 2020; Prisle, 2021; Vepsäläinen et al., 2022, 2023). For spherical droplets of diameter D_{wet}=0.1, 1, and 10 µm, the surface area to bulk volume ratio ($A/V = 6/d$) is 60, 6, and 0.6 $\mu\mathrm{m}^{-1}$, respectively (Prisle et al., 2010). Given the high A/V of small droplets, such as submicron activating aqueous aerosols, and the surface propensity of atmospherically relevant organic acids, surface specific properties may significantly contribute to, or entirely dominate, the overall aerosol properties (Prisle et al., 2012b; Prisle, 2021).

Werner et al. (2018) investigated the surface characteristics of butyric and pentanoic acid in dilute aqueous solution (50 mM carboxylic acid) using surface-sensitive X-ray Photoelectron Spectroscopy, and found that the acid-base equilibrium was systematically shifted in the surface, corresponding to an apparent shift in pK_a of the order of 1 to 2 pH units, compared to the bulk solution. Similar magnitudes of apparent pK_a shift were also previously observed by Prisle et al. (2012b) for dilute aqueous mixtures of decanoate/decanoic acid and by Öhrwall et al. (2015) for propanoic and octanoic acid solutions. Each of these organic acids showed significant surface propensity in the aqueous solutions. Here, we introduce a simple implementation of the surface specific shift in acid/base equilibrium reported in these studies. We introduce acidity in the whole aerosol using α, and modulate its value to represent observations made in the surface.

The pK_a are derived by taking the negative logarithm of the acid dissociation constant from eq. 24, and the pK_a^{bulk} and apparent pK_a at the surface, pK_a^{surf}, are related as

$$pK_a^{\mathrm{surf}} = pK_a^{\mathrm{bulk}} + \log\left(\frac{\gamma_{\mathrm{H_3O^+}}\gamma_{\mathrm{A^-}}}{\gamma_{\mathrm{HA}}}\right), \tag{34}$$

where γ_i denotes the activity coefficient of an ideal dilute 1 molar solution of component i. The observed shift in apparent pK_a in the surface can be rationalized in terms of the factor $\log\left(\frac{\gamma_{\mathrm{H_3O^+}}\gamma_{\mathrm{A^-}}}{\gamma_{\mathrm{HA}}}\right)$, reflecting the increased non-ideality of the charged deprotonated species ($\mathrm{A^-}$) and hydronium ions, compared to the neutral molecular acid (HA), in the surface. The magnitude of the 1 – 2 pH units shift in $\log\left(\frac{\gamma_{\mathrm{H_3O^+}}\gamma_{\mathrm{A^-}}}{\gamma_{\mathrm{HA}}}\right)$ further depends on the increased concentrations of the organic acid conjugate pair in the surface driven by bulk-surface partitioning (Prisle et al., 2012b; Öhrwall et al., 2015; Werner et al., 2018).

We here consider two values of the apparent shift, covering the range of observations, and representing stronger or less strong influence of surface properties on the whole droplet. For the monoprotic acid, pK_a^{bulk}+1 and pK_a^{bulk}+2 were extrapolated from the reported pK_a. To represent the surface shifted dissociation of both carboxylic groups in the diprotic acid, we increase both the first and second pK_a by one pH unit for pK_a^{bulk}+1, and by two pH units for pK_a^{bulk}+2. For each of the apparent pK_a, the corresponding dissociation degree (α) is calculated for the monoprotic acid using eq. 28 and for the diprotic acid using eq. 31. α is smaller with increasing pK_a, and therefore the shifted acidity in the surface represents suppressed organic dissociation. The van't Hoff factor is calculated for each apparent pK_a using eq. 32. The dissociation degrees and van't Hoff factors for the

https://doi.org/10.5194/egusphere-2023-438
Preprint. Discussion started: 28 March 2023

no organic dissociation (no diss), bulk organic dissociation (pK_a^{bulk}) and surface modulated suppressed organic dissociation (pK_a^{bulk}+1 and pK_a^{bulk}+2), for all the OA mass fractions considered here are given in the appendix (Table A1).

We use two different organic acids as examples, malonic acid (a diprotic acid) and decanoic acid (a monoprotic acid), as they are important aerosol components in the atmosphere (Narukawa et al., 2002; Tedetti et al., 2006; Prisle et al., 2012b) and prominent examples of moderately and strongly surface active species, respectively (Vepsäläinen et al., 2022). The molecular weight, density and pK_a^{bulk} values available from literature, as well as the surface modulated pK_a^{bulk}+1 and pK_a^{bulk}+2, for decanoic acid and malonic acid, are given in Table 3.

Table 3. Properties of the organic acids used in all model simulations of the organic acids.

	Malonic acid	Decanoic acid
Molecular weight	104 gmol^{-1}	172.26 gmol^{-1}
Density, ρ	1.62 gcm^{-3}	0.893 gcm^{-3}
pK_{a1}	2.8[a]	4.9[b]
pK_{a2}	5.7[a]	-
pK_a^{bulk}	8.5	4.9
pK_a^{bulk}+1	10.5	5.9
pK_a^{bulk}+2	12.5	6.9

[a] Stahl and Wermuth (2002). [b] Martell and Smith (1974).

3 Results and discussions

We present the results of the HAMBOX-sulfur chemistry calculations in terms of total hydrogen ion concentration, $[\mathrm{H}^+]_{\mathrm{tot}}$, and total sulfate concentration, $[\mathrm{SO}_4^{2-}]$, in the aerosol population, accounting for bulk organic dissociation, surface modulated suppressed organic dissociation and no organic dissociation. The consecutive effect on cloud activating properties, in terms of change in CDNC ($\Delta\mathrm{CDNC}$) and RE, compared to no organic dissociation is then presented for bulk dissociation and surface modulated suppressed dissociation of the organics.

https://doi.org/10.5194/egusphere-2023-438
Preprint. Discussion started: 28 March 2023

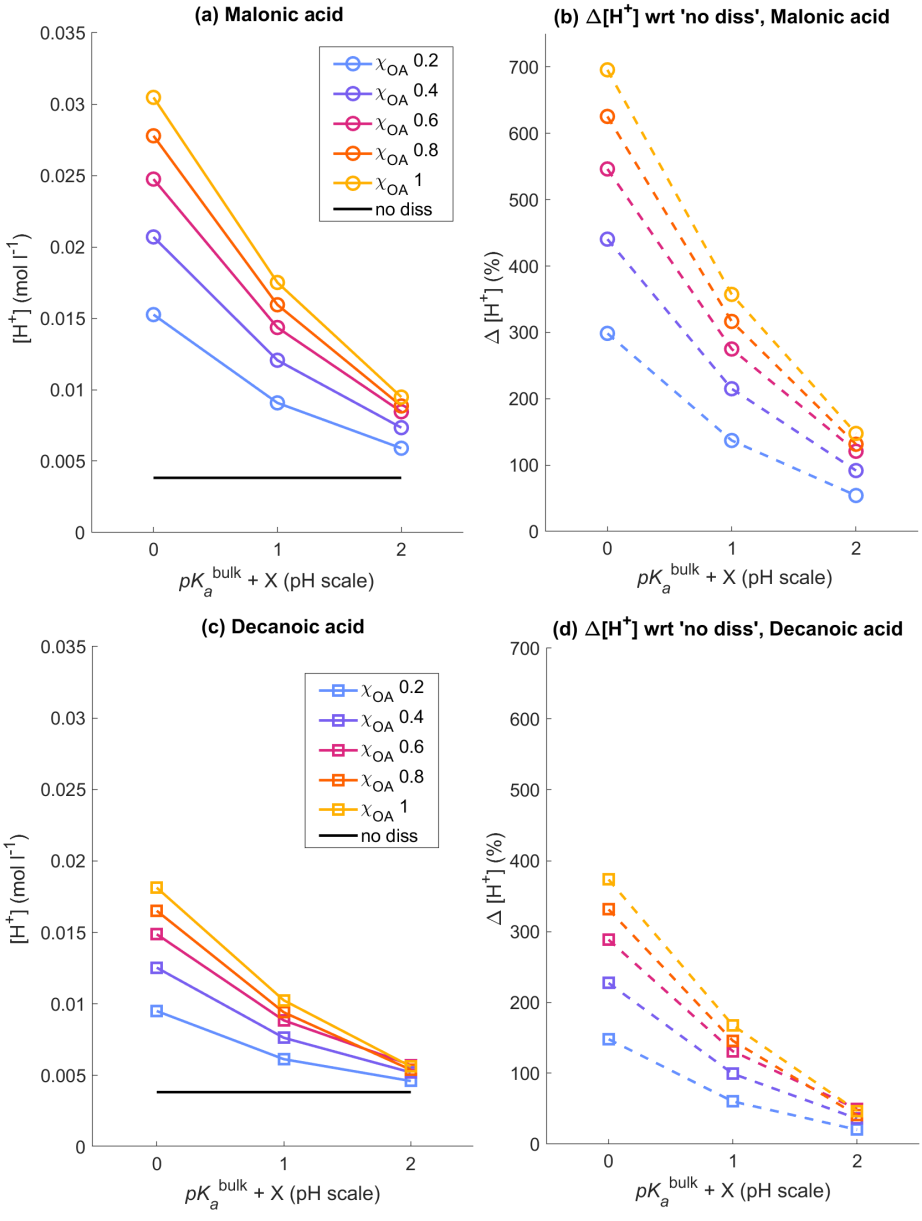

Figure 1. Aqueous aerosol hydrogen ion concentration, $[\mathrm{H}^+]_{\mathrm{tot}}$, calculated with the sulfur chemistry module of HAMBOX for the whole aerosol population with droplet radius 0.317 µm to 40 µm, after 1 hour of simulation time, assuming five different initial organic mass fractions ($\chi_{\mathrm{OA}} = \{0.2, 1\}$), denoted by different colors (see also Table 2), from equation 20 with varying apparent pK_a = pK_a^{bulk}+X, corresponding to representations of bulk (X=0) and surface modulated (X=1 and X=2) organic dissociation. (a, b) All OA is assumed as Malonic acid. (c, d) All OA is assumed as Decanoic acid. The 'no diss' represents simulation without accounting for organic dissociation, and sub-figures b and d show the relative change in $[\mathrm{H}^+]$ with respect to the 'no diss', $\Delta\,[\mathrm{H}^+]$, calculated using eq. 21.

https://doi.org/10.5194/egusphere-2023-438
Preprint. Discussion started: 28 March 2023

Figure 1 shows the aqueous aerosol hydrogen ion concentration ($[H^+]_{tot}$) calculated with HAMBOX using eq. 20 as a function of varying apparent pK_a = pK_a^{bulk}+X, corresponding to representations of bulk (X=0) and surface modulated (X=1 and 2) organic dissociation, considering (a,b) OA = malonic acid, and (c,d) OA = decanoic acid, for varying initial mass fraction of organic aerosol ($\chi_{OA} = \{0.2, 1\}$ in different colours). The hydrogen ion concentration with no organic dissociation (obtained using eq. 19) is also shown as a black line. As expected, the hydrogen ion concentration in the aerosol does not change with apparent pK_a when organic dissociation is not accounted for, whereas a significant increase in hydrogen ion concentration is observed when organic dissociation is considered for both organic acids. The hydrogen ion concentration is highest when bulk organic dissociation is considered (pK_a^{bulk}) for all initial OA mass fractions, and decreases as OA dissociation is increasingly suppressed according to the surface modulated acidity in the form of increasing apparent pK_a. The relative change in hydrogen ion concentration compared to 'no diss' ($\Delta[H^+]$) for malonic acid is 298.5% with pK_a^{bulk} for the lowest OA mass fraction (χ_{OA} 0.2) and 696% for the highest OA mass fraction (χ_{OA} 1). Under surface modulated suppressed organic dissociation of pK_a^{bulk}+1, the $\Delta[H^+]$ decreases to 137% and 357%, respectively, for χ_{OA} 0.2 and χ_{OA} 1. On further suppression of organic dissociation with pK_a^{bulk}+2, these values further decrease to 54% and 148%, respectively. The hydrogen ion concentration for decanoic acid at pK_a^{bulk}, increases by 148% with respect to 'no diss' for χ_{OA} 0.2 and by 374% for χ_{OA} 1. At pK_a^{bulk}+1, these values decrease to 61% and 168%, respectively, and at pK_a^{bulk}+2, they further decrease to 20% and 47% for χ_{OA} 0.2 and 1, respectively. Therefore, on considering stronger surface modulated suppression of organic dissociation with pK_a^{bulk}+2, the total hydrogen ion concentration in the aqueous aerosol is still 20 to 47% higher than 'no diss' for decanoic acid, and 54 to 148% for malonic acid, depending on the initial organic mass fraction.

https://doi.org/10.5194/egusphere-2023-438
Preprint. Discussion started: 28 March 2023

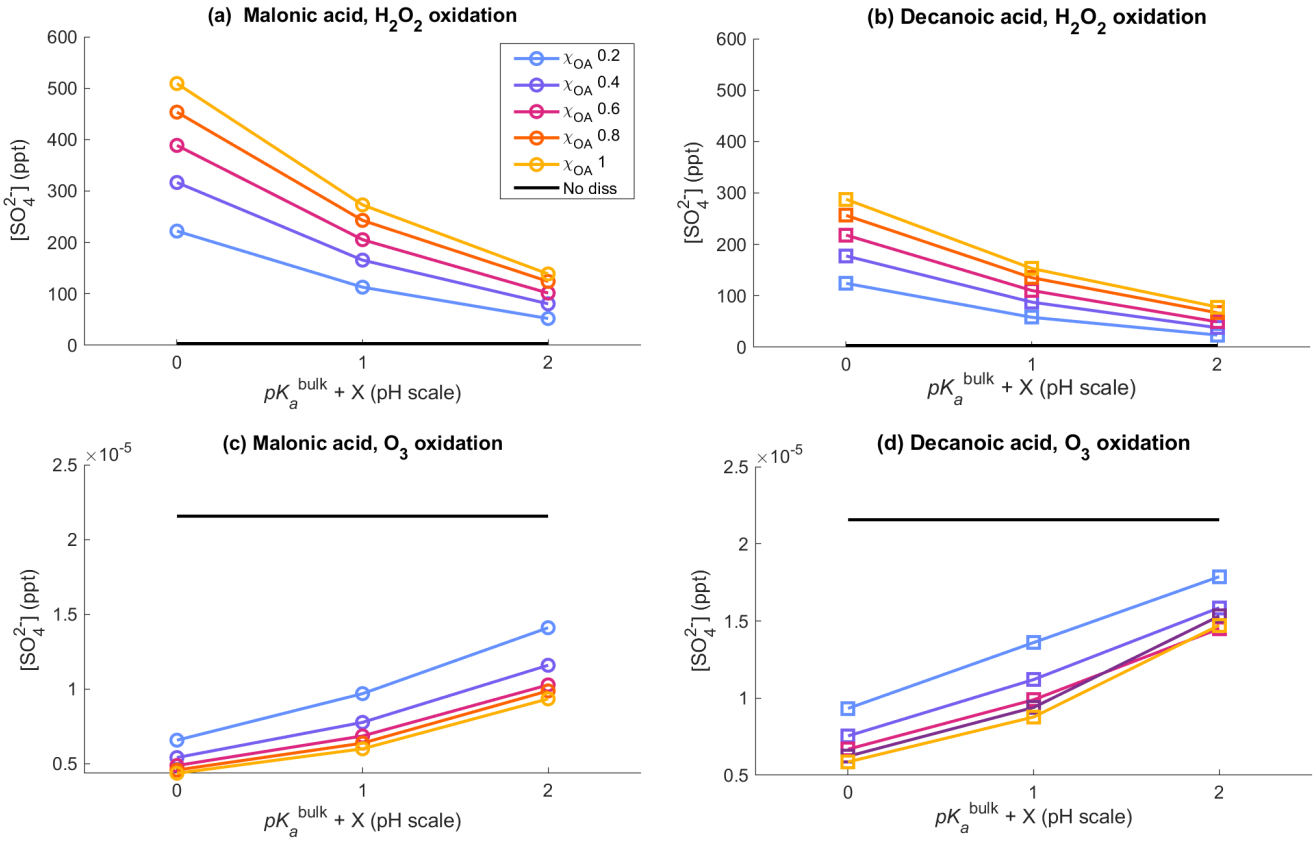

Figure 2. Aqueous aerosol sulfate concentrations ($[SO_4^{2-}]$) for malonic acid (sub-figures a, c) and decanoic acid (sub-figures b, d), obtained from oxidation of sulfur dioxide by H_2O_2 (using eq. 15 and 13) and O_3 (using eq. 16), as a function of varying apparent pK_a^{bulk}+X, corresponding to representations of bulk (X=0) and surface modulated (X=1 and 2) organic dissociation, calculated in the sulfur chemistry module of HAMBOX for the whole aerosol population with droplet radius 0.317 µm to 40 µm, after 1 hour of simulation time, assuming five different initial organic mass fractions (χ_{OA}), denoted by different colors (see also Table 2). The 'no diss' represents simulation without accounting for organic dissociation.

Figure 2 shows the sulfate concentrations ($[SO_4^{2-}]$) produced through oxidation of SO_2 by H_2O_2 and O_3 (Section 2.3) for the whole aerosol population with droplet radius 0.317 µm to 40 µm, after 1 hour of simulation time, for varying bulk and surface modulated pK_a of OA dissociation, where OA= malonic acid (sub-figures a, c) and decanoic acid (sub-figures b, d), assuming five different initial organic mass fractions ($\chi_{\mathrm{OA}} = \{0.2, 1\}$), denoted by different colors. The total sulfate
330 concentration obtained from 'no diss' is shown as a black line for reference. The relative changes in the sulfate concentration compared to 'no diss' ($\Delta[SO_4^{2-}]$), for both oxidation pathways are given in the appendix (fig. A1). Sulfate concentration from H_2O_2 oxidation increases drastically for both organic acids when organic dissociation is accounted for. From eq. 15, it may seem that sulphate concentration should decrease with increasing $[H^+]_{\mathrm{tot}}$ concentration, but the reverse is observed in figure

https://doi.org/10.5194/egusphere-2023-438
Preprint. Discussion started: 28 March 2023

2. This is a property of the general acid catalysed mechanism, where the pK_a dependent k_{HA} offsets the decrease in sulphate concentration caused by increased $[\mathrm{H^+}]_{\mathrm{tot}}$ concentration. These results are in line with Liu et al. (2020) where the general acid catalysed $\mathrm{H_2O_2}$ oxidation was suggested as a source to explain 'missing' sulfate during severe haze episodes. The oxidation of $\mathrm{SO_2}$ by $\mathrm{O_3}$ follows a straightforward dependence on $[\mathrm{H^+}]_{\mathrm{tot}}$ concentration from eq. 16, where increased hydrogen ion concentration results in decreased $[\mathrm{SO_4^{2-}}]$, compared to 'no diss'.

For malonic acid, $\mathrm{H_2O_2}$ oxidation shows an increase in total sulfate concentration compared to 'no diss', with $\Delta[\mathrm{SO_4^{2-}}]$ ranging from 6434% to 14876% at pK_a^{bulk} with increasing $\chi_{\mathrm{OA}} = \{0.2, 1\}$. With surface modulated suppressed organic dissociation, $[\mathrm{SO_4^{2-}}]$ decreases compared to pK_a^{bulk}. The lowest simulated $\Delta[\mathrm{SO_4^{2-}}]$ is observed for pK_a^{bulk}+2 and χ_{OA} 0.2. But even at this point, $\Delta[\mathrm{SO_4^{2-}}]$ is 1432%, which is a significant increase compared to 'no diss'. Similar trends are observed for the $\mathrm{H_2O_2}$ oxidation with decanoic acid (sub-figure b), where the highest sulfate concentration is obtained for bulk organic dissociation, pK_a^{bulk} with $\Delta[\mathrm{SO_4^{2-}}]$ ranging from 3557 to 8367% corresponding to $\chi_{\mathrm{OA}} = \{0.2, 1\}$. The lowest sulfate concentration predicted for OA=decanoic acid is as expected for the stronger surface modulated suppression of organic dissociation at pK_a^{bulk}+2 and χ_{OA} 0.2, with $\Delta[\mathrm{SO_4^{2-}}]$ at this point being 598%. The sulfate concentration from $\mathrm{O_3}$ oxidation decreases by 70 to 80% compared to 'no diss' for OA=malonic acid at pK_a^{bulk} with increasing $\chi_{\mathrm{OA}} = \{0.2, 1\}$. The decrease is less for surface modulated suppressed dissociation, as expected, and is 35 to 55% for the stronger dissociation suppression at pK_a^{bulk}+2. OA=decanoic acid also shows a similar trend for sulfate concentration from $\mathrm{O_3}$ oxidation, where decrease in sulfate concentration is in the range of 20 to 75% for bulk and surface OA dissociation. Therefore, the $\mathrm{H_2O_2}$ oxidation of $\mathrm{SO_2}$ results in a far greater increase in $[\mathrm{SO_4^{2-}}]$ in the total aerosol population than the decrease in $[\mathrm{SO_4^{2-}}]$ from the $\mathrm{O_3}$ oxidation of $\mathrm{SO_2}$, compared to 'no diss'.

Thus, the $[\mathrm{H^+}]_{\mathrm{tot}}$ increase when OA acidity and ensuing dissociation is accounted for also translates into significant increase in predicted sulfate concentration, $[\mathrm{SO_4^{2-}}]$, in the aqueous aerosol. As expected, the effect is smaller when organic dissociation is suppressed with surface modulated pK_a, but even for the stronger suppression, the effect is 1432–4000% and 598–2500% with $\chi_{\mathrm{OA}} = \{0.2, 1\}$, for malonic acid and decanoic acid, respectively. We see that the effect is larger for the $\mathrm{H_2O_2}$ oxidation, suggesting that this pathway is more sensitive to inclusion of acidity and dissociation effects.

https://doi.org/10.5194/egusphere-2023-438
Preprint. Discussion started: 28 March 2023

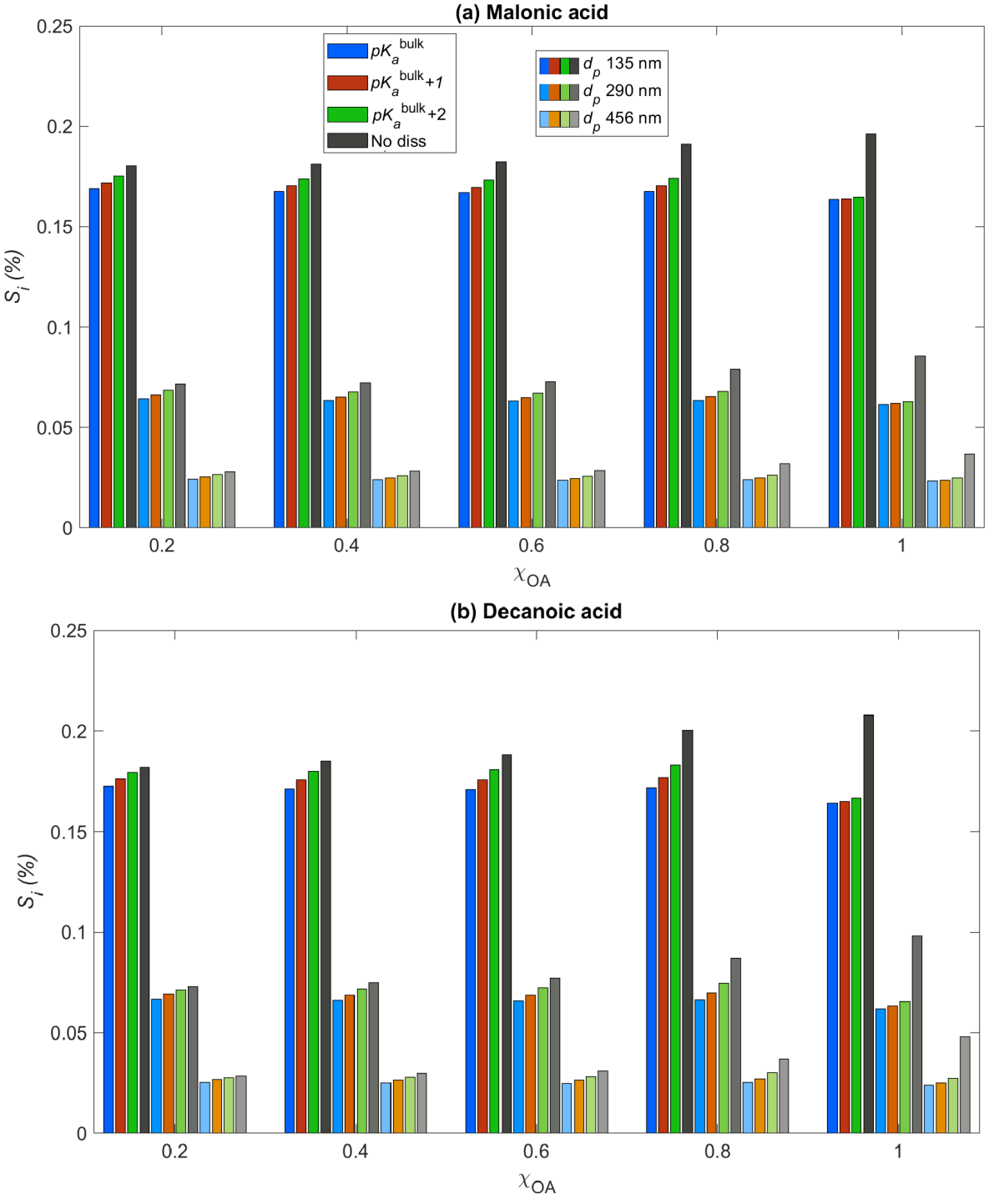

Figure 3. Critical supersaturation (S_i) as a function of the initial organic mass fraction (χ_{OA}) calculated using eq. 3 for (a) malonic acid and (b) decanoic acid, for three initial dry particle sizes (d_p = 135 nm, 290 nm and 456 nm) and apparent pK_a representing bulk (pK_a^{bulk}) and surface (pK_a^{bulk}+1 and pK_a^{bulk}+2) organic dissociation. The 'no diss' represents simulation without accounting for organic dissociation.

https://doi.org/10.5194/egusphere-2023-438
Preprint. Discussion started: 28 March 2023

Figure 3 shows the critical supersaturation predicted with HAMBOX for the five selected initial organic mass fractions (χ_{OA}), obtained for three dry particle sizes, d_p = 135 nm (darkest shade), 290 nm (lighter shade) and 456 nm (lightest shade), with apparent pK_a = pK_a^{bulk}+X, corresponding to representations of bulk (X=0, blue) and surface modulated (X=1, red and X=2, green) organic dissociation, considering (a) OA = malonic acid, and (b) OA = decanoic acid. The 'no diss' condition is also shown (black bars) for each dry particle size in both figures. The aerosol size redistribution caused by the increased sulfate concentrations affects the calculation of the droplet radius (D_{wet}) in eq. 3 and thus, the critical supersaturation is affected by bulk (pK_a^{bulk}) and surface modulated (pK_a^{bulk}+1 and pK_a^{bulk}+2) dissociation of the OA. We see that for both organic acids, the increased sulfate concentrations in the aqueous aerosols, compared to 'no diss', is sufficient to significantly decrease the critical supersaturation for all three dry particle sizes and all OA mass fractions considered. As expected, the decrease in S_i is lesser when surface modulated suppressed dissociation is considered. For decanoic acid, the difference between the S_i calculated for bulk and surface apparent (pK_a) is larger than those calculated for malonic acid. This difference is more visible in the higher dry particle sizes (lightest shade) and higher organic mass fraction (χ_{OA} 0.6 to 1). This suggests that the simulated S_i from decanoic acid dissociation is more susceptible to changes in the surface shifted apparent (pK_a) than malonic acid, especially at higher dry particle sizes and higher organic mass fractions. As the χ_{OA} increases, the difference in S_i between all apparent pK_a and 'no diss' increases for both organic acids. As the calculated S_i in each bin also reflects the changes in the water activity due to organic dissociation (section 2.4.3), we see that for both organic acids, the water activity is sufficiently reduced, even for the surface modulated suppressed dissociation, to significantly decrease S_i, compared to 'no diss'. It is well known that critical supersaturation increases with increasing OA due to hygroscopicity (Svenningsson et al., 2006), however, fig. 3 shows that organic dissociation can partially counter this increase. This effect is smaller if surface modulated suppressed organic dissociation is considered, which is more relevant in smaller droplets and particles due to the high surface-to-bulk ratio (Prisle, 2021).

https://doi.org/10.5194/egusphere-2023-438
Preprint. Discussion started: 28 March 2023

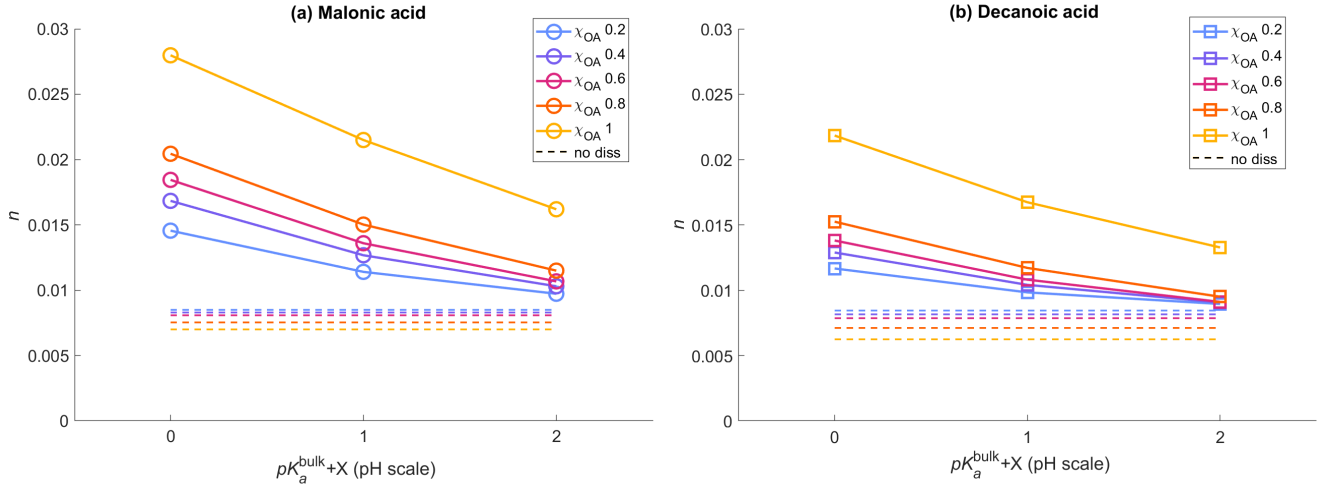

Figure 4. The average activated fraction (n) in the whole aerosol population with droplet radius 0.317 µm to 40 µm, after 1 hour of simulation time, assuming five different initial organic mass fractions (χ_{OA}), denoted by different colors, calculated using eq. 8 corresponding to representations of bulk and surface modulated organic dissociation, considering (a) OA = malonic acid, and (b) OA = decanoic acid. The 'no diss' average activated fraction for each χ_{OA} is shown as a dashed line in corresponding colors.

Figure 4 shows the activated fraction (n) averaged for all size bins calculated for initial organic mass fractions, $\chi_{\mathrm{OA}} = \{0.2, 1\}$, shown by different colours, calculated using eq. 8, with apparent $pK_a = pK_a^{\mathrm{bulk}}$+X, corresponding to representations of bulk (X=0) and surface modulated (X=1 and 2) organic dissociation, considering (a) OA = malonic acid, and (b) OA = decanoic acid. The 'no diss' average activated fraction, shown in corresponding colors as dashed lines, approximately 0.006–0.008 for both organic acids, with $\chi_{\mathrm{OA}} = \{0.2, 1\}$. The inclusion of organic dissociation effects in the calculations results in a higher activated fraction than 'no diss', for both the organic acids, with malonic acid dissociation resulting in a greater n than decanoic acid dissociation under the same χ_{OA} and apparent pK_a. This is expected as malonic acid is a stronger acid with lower pK_a and $[\mathrm{H}^+]_{\mathrm{tot}}$ from malonic acid dissociation under the same conditions was higher than that from decanoic acid dissociation. The maximum activated fraction is observed for pK_a^{bulk}, 0.014 to 0.027 for OA = malonic acid and 0.012 to 0.021 for OA = decanoic acid. For surface modulated suppressed organic dissociation, pK_a^{bulk}+1, the activated fraction decreases to 0.011–0.021 and 0.010–0.016 for OA = malonic and decanoic acids, respectively. As expected, for the stronger surface modulated dissociation suppression, pK_a^{bulk}+2, the activated fraction further decreases, but is still higher than 'no diss' (0.009–0.016 and 0.009–0.013 for OA = malonic and decanoic acids, respectively, corresponding to $\chi_{\mathrm{OA}} = \{0.2, 1\}$). For both organic acids, the activated fraction also increases with increasing χ_{OA}, which is expected as the $[\mathrm{H}^+]_{\mathrm{tot}}$ increases with increasing χ_{OA}. For both the organic acids, the amount of $[\mathrm{H}^+]_{\mathrm{tot}}$ is sufficient to decrease the critical supersaturation enough to translate into an increased activated fraction for both bulk and surface modulated suppressed organic dissociation, with the effect being smaller for the suppressed dissociation, as expected.

https://doi.org/10.5194/egusphere-2023-438
Preprint. Discussion started: 28 March 2023

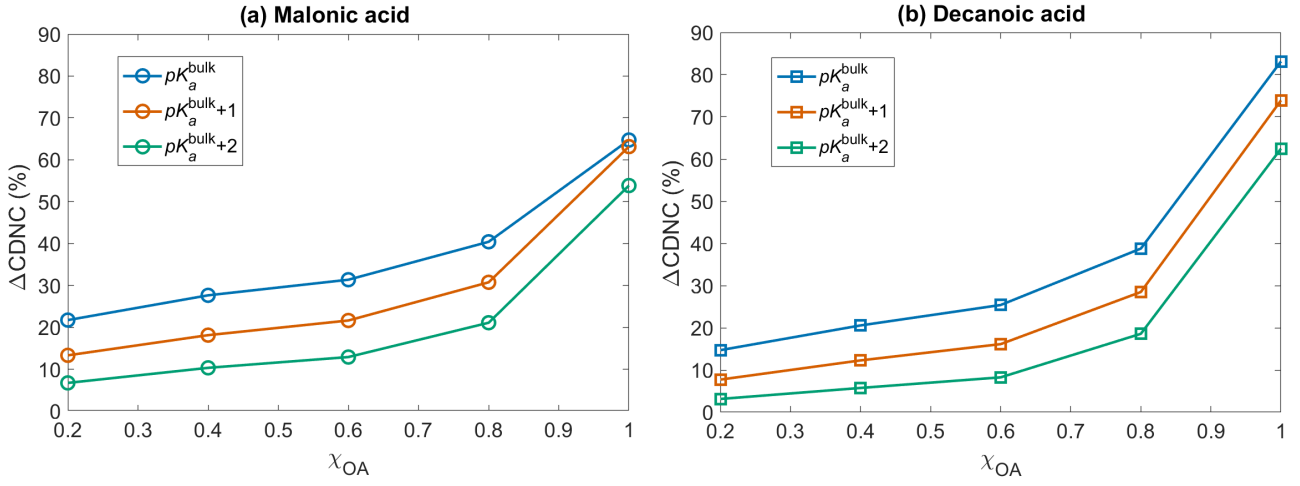

Figure 5. The change in cloud droplet number concentration (ΔCDNC, calculated using equation 10) with respect to 'no diss' for (a) OA = malonic acid and (b) OA = decanoic acid, calculated using equation 10 for the five selected initial organic mass fractions (χ_{OA}) assuming organic dissociation in the bulk (pK_a^{bulk}, blue) and surface modulated organic dissociation (pK_a^{bulk}+1, orange and pK_a^{bulk}+2, green).

Figure 5 shows the CDNC enhancement (ΔCDNC) with respect to 'no diss' for the five selected initial organic mass fraction, $\chi_{\mathrm{OA}} = \{0.2, 1\}$, for (a) malonic acid and (b) decanoic acid, considering the three representations of organic dissociation with apparent pK_a at pK_a^{bulk} (blue), pK_a^{bulk}+1 (orange) and pK_a^{bulk}+2 (green). A significant enhancement in CDNC is seen for both malonic and decanoic acid OA, compared to when no organic acid dissociation is considered ('no diss'). Similar trends are seen for both acids, where pK_a^{bulk} shows the highest CDNC enhancement compared to 'no diss'. This is expected based on the calculated $[\mathrm{H}^+]_{\mathrm{tot}}$ and $[\mathrm{SO}_4^{2-}]$ from the bulk OA dissociation and surface modulated suppressed OA dissociation and consequent critical supersaturation (S_i) from both organic acids. At the bulk pK_a, ΔCDNC for decanoic acid ranges from 14.70% to 83.14% on increasing $\chi_{\mathrm{OA}} = \{0.2, 1\}$. For the malonic acid, the ΔCDNC is smaller ranging from 21.73% to 64.72% for a corresponding increase in χ_{OA} at bulk apparent pK_a. Under surface modulated suppressed dissociation of pK_a^{bulk}+1, the CDNC enhancement is less than that obtained from pK_a^{bulk}, ranging from 7.73% to 73.9% for decanoic acid and 13.31% to 63.15% for malonic acid. For the stronger surface modulated dissociation suppression, pK_a^{bulk}+2, the CDNC enhancement with respect to 'no diss' is 3.14% to 62.47% for decanoic acid and 6.72% to 53.85% for malonic acid, for $\chi_{\mathrm{OA}} = \{0.2, 1\}$.

The CDNC enhancement upon including OA acidity is caused by the change in size distribution due to the increased sulfate concentrations, which shifts the size distribution towards larger particles, which are more effective in CDNC production (Hudson and Da, 1996; McFiggans et al., 2006). Since size plays a significant role in cloud-nucleating ability of aerosol particles (Dusek et al., 2006), the effect of organic dissociation on cloud response will be different depending on whether bulk or surface properties are used to describe the organic aerosol, and from fig. 5 we see that this difference is significant for both malonic and decanoic acid under the simulation conditions. The size distribution after one hour of simulation time with and without activating the sulfur chemistry module, for OA = malonic acid and decanoic acid considering χ_{OA} = 0.8 with apparent

https://doi.org/10.5194/egusphere-2023-438
Preprint. Discussion started: 28 March 2023

pK_a corresponding to bulk organic dissociation, surface modulated suppressed dissociation and no dissociation, is shown in the appendix (figures A2 and A3). For 'no diss', the size distribution is almost similar at one hour for simulations with and without activating the sulfur chemistry module, for both organic acids. For organic dissociation at pK_a^{bulk}, the size distribution is significantly different from the 'no diss' size distribution, at one hour. The change is smaller for the suppressed organic dissociation at pK_a^{bulk}+1 and pK_a^{bulk}+2, however the change in size distribution even from the stronger suppressed dissociation is significant enough to effect 6.7–53.8 % and 3.1–62.4 % ΔCDNC for OA = malonic acid and decanoic acid, respectively, compared to 'no diss'.

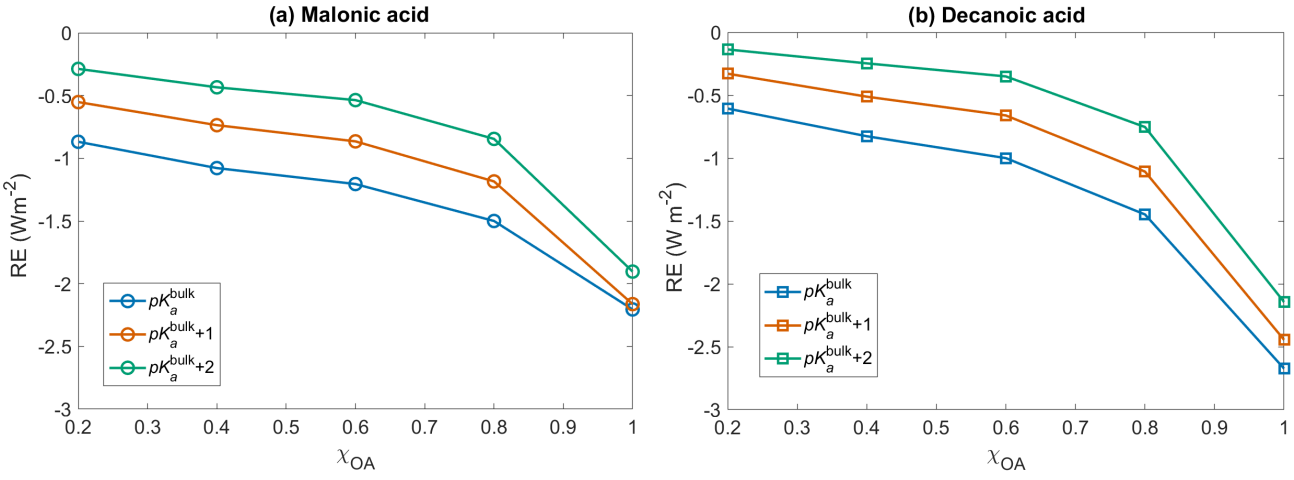

Figure 6. The short wave radiative effect (RE, calculated using equation 12) with respect to 'no diss' for (a) malonic acid and (b) decanoic acid, for the five selected initial organic mass fractions (χ_{OA}) assuming organic dissociation in the bulk (pK_a^{bulk}, blue) and surface modulated organic dissociation (pK_a^{bulk}+1, orange and pK_a^{bulk}+2, green).

Figure 6 shows the short-wave radiative effect (RE) with respect to 'no diss' for the five selected initial organic mass fractions, $\chi_{\text{OA}} = \{0.2, 1\}$, considering the entire organic fraction as (a) malonic acid and (b) decanoic acid, for representations of bulk organic dissociation, pK_a^{bulk} (blue), and surface modulated suppressed organic dissociation, pK_a^{bulk}+1 (orange) and pK_a^{bulk}+2(green). The inclusion of organic acid dissociation leads to a cooling effect for both organic acids, compared to 'no diss'. Considering organic dissociation with bulk properties with apparent pK_a at pK_a^{bulk}, the highest cooling effect is observed for both acids, ranging from - 0.6 Wm^{-2} to - 2.7 Wm^{-2} for decanoic acid and - 0.86 Wm^{-2} to - 2.2 Wm^{-2} for malonic acid as χ_{OA} increases from 0.2 to 1. The effect is smaller when considering surface modulated suppressed dissociation, but still significant compared to 'no diss', with RE ranging from -0.5 Wm^{-2} to -2.2 Wm^{-2} for malonic acid and -0.3 Wm^{-2} to -2.4 Wm^{-2} for decanoic acid at pK_a^{bulk}+1 and -0.3 Wm^{-2} to -1.6 Wm^{-2} for malonic acid and -0.1 Wm^{-2} to -2.1 Wm^{-2} for decanoic acid at pK_a^{bulk}+2.

Overall, our results show that dissociation of organic aerosols in the aqueous phase, exemplified with common atmospheric OA moderately strong acids malonic and decanoic acid, can influence the aqueous sulfur chemistry to have a significant

https://doi.org/10.5194/egusphere-2023-438
Preprint. Discussion started: 28 March 2023

effect on the cloud short-wave radiative effect. A surface-modulated shifted acid-base equilibrium can change the extent to which these organic acids dissociate and therefore, the concentration of hydrogen ions at the surface is different than what is immediately expected from the bulk pH. Under these conditions, the effect of organic dissociation on the cloud properties are reduced, but still significant. Since many atmospheric OA are acidic, this may be important to represent in large scale models. The effect of surface modulated suppressed dissociation in the atmosphere will depend on aerosol and droplet size and is expected to be especially relevant for smaller aerosol sizes, and our results suggest that OA dissociation should not be omitted for accurate predictions involving organic aerosols.

4 Conclusion

We investigated the effects of organic aerosol dissociation on total hydrogen ion concentration in aqueous aerosols and the impact on resulting secondary sulfate aerosol mass, cloud droplet number concentration, and aerosol short-wave radiative effect, using the aerosol–chemistry-climate box model ECHAM6.3–HAM2.3. Simulations were carried out considering the entire OA to comprise organic acid and used malonic and decanoic acid as proxies for atmospheric OA acids. Dissociation of organic acids was considered in three scenarios: 1) the current standard of no dissociation, 2) following well-known bulk solution properties given by the reported acid constant pK_a, and 3) accounting for a surface-modulated suppression of dissociation as observed in recent laboratory experiments.

Our results show that organic dissociation increases hydrogen ion concentrations in the aqueous aerosol phase, as expected. This leads to strongly increased secondary sulfate aerosol mass, which in turn decreases the critical supersaturation for cloud droplet activation and a higher activated fraction is obtained than if OA dissociation is not considered. The cloud response is observed as enhanced cloud droplet number concentration and a strong short-wave radiative effect of clouds. The effects of dissociation are greatest when considering the bulk acidity of OA, but still significant even when potential surface-modulated suppression is also included.

As many atmospheric organic aerosol components are acidic (Pye et al., 2020), and thereby can have significant impacts on cloud properties, this work highlights the importance of including effects of organic dissociation in large scale atmospheric models. We suspect that, combined with the high surface to bulk ratio and surface-bulk partitioning in small droplets, the effects of organic dissociation and potential size dependent surface modulated dissociation could be significant in explaining some knowledge gaps about organic acidity in atmospheric aerosols. Additionally, OA dissociation could be particularly relevant in explaining discrepancies of atmospheric models with observations for polluted environments (Lee et al., 2013) where organic mass fraction is usually high and the organic dissociation effects could become more significant. Many of these organic aerosol acids may also be surface active in aqueous solutions (Gérard et al., 2019), such as activating droplets, and therefore corrections to account for surface modulated suppression of organic dissociation may also be necessary. This is expected to be particularly important for smaller size ranges, due to the high surface-to-bulk ratio of such aerosols (Bzdek et al., 2020; Prisle, 2021).

https://doi.org/10.5194/egusphere-2023-438
Preprint. Discussion started: 28 March 2023

Code and data availability. Code and underlying simulation data are available upon request from the corresponding author.

Appendix A

Table A1. The OA van't Hoff factor (i_{OA}) calculated using eq. 32 and dissociation degree (α, in parenthesis) calculated using eq. 28 and 31 for decanoic acid and malonic acid, respectively, corresponding to the apparent pK_a for bulk organic dissociation (pK_a^{bulk}) and surface suppressed organic dissociation (pK_a^{bulk}+1 and pK_a^{bulk}+2) for the chosen organic mass fractions.

Malonic acid				
χ_{OA}	i_{OA} (α), pK_a^{bulk}	i_{OA} (α), pK_a^{bulk}+1	i_{OA} (α), pK_a^{bulk}+2	i_{OA} (α), no diss
0.2	2.12 (0.560)	1.90 (0.450)	1.70 (0.350)	1 (0)
0.4	2.064 (0.532)	1.85 (0.425)	1.66 (0.331)	1 (0)
0.6	2.02 (0.510)	1.81 (0.405)	1.63 (0.315)	1 (0)
0.8	1.996 (0.498)	1.770 (0.385)	1.590 (0.295)	1 (0)
1	1.960 (0.480)	1.720 (0.360)	1.560 (0.280)	1 (0)
Decanoic acid				
χ_{OA}	i_{OA} (α), pK_a^{bulk}	i_{OA} (α), pK_a^{bulk}+1	i_{OA} (α), pK_a^{bulk}+2	i_{OA} (α), no diss
0.2	1.993 (0.993)	1.905 (0.905)	1.720 (0.720)	1 (0)
0.4	1.989 (0.989)	1.890 (0.890)	1.715 (0.715)	1 (0)
0.6	1.985 (0.985)	1.875 (0.875)	1.705 (0.705)	1 (0)
0.8	1.981 (0.981)	1.845 (0.845)	1.680 (0.680)	1 (0)
1	1.978 (0.978)	1.823 (0.823)	1.650 (0.650)	1 (0)

https://doi.org/10.5194/egusphere-2023-438
Preprint. Discussion started: 28 March 2023

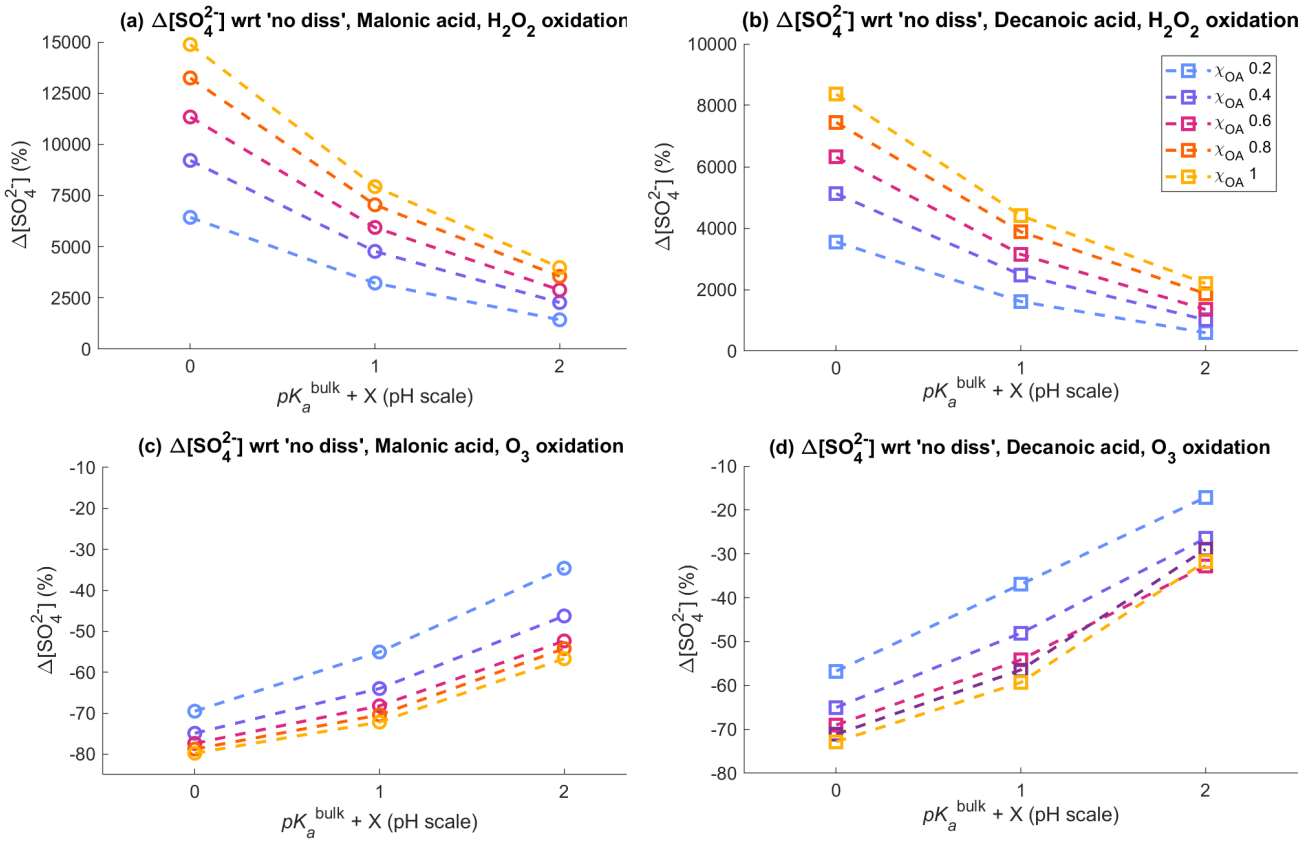

Figure A1. The relative change of sulfate concentrations ($\Delta[SO_4^{2-}]$, calculated using equation 22) with respect to 'no OA dissociation' where organic dissociation is not considered is shown in sub-figures b and d for the H_2O_2 and O_3 pathways respectively.

https://doi.org/10.5194/egusphere-2023-438
Preprint. Discussion started: 28 March 2023

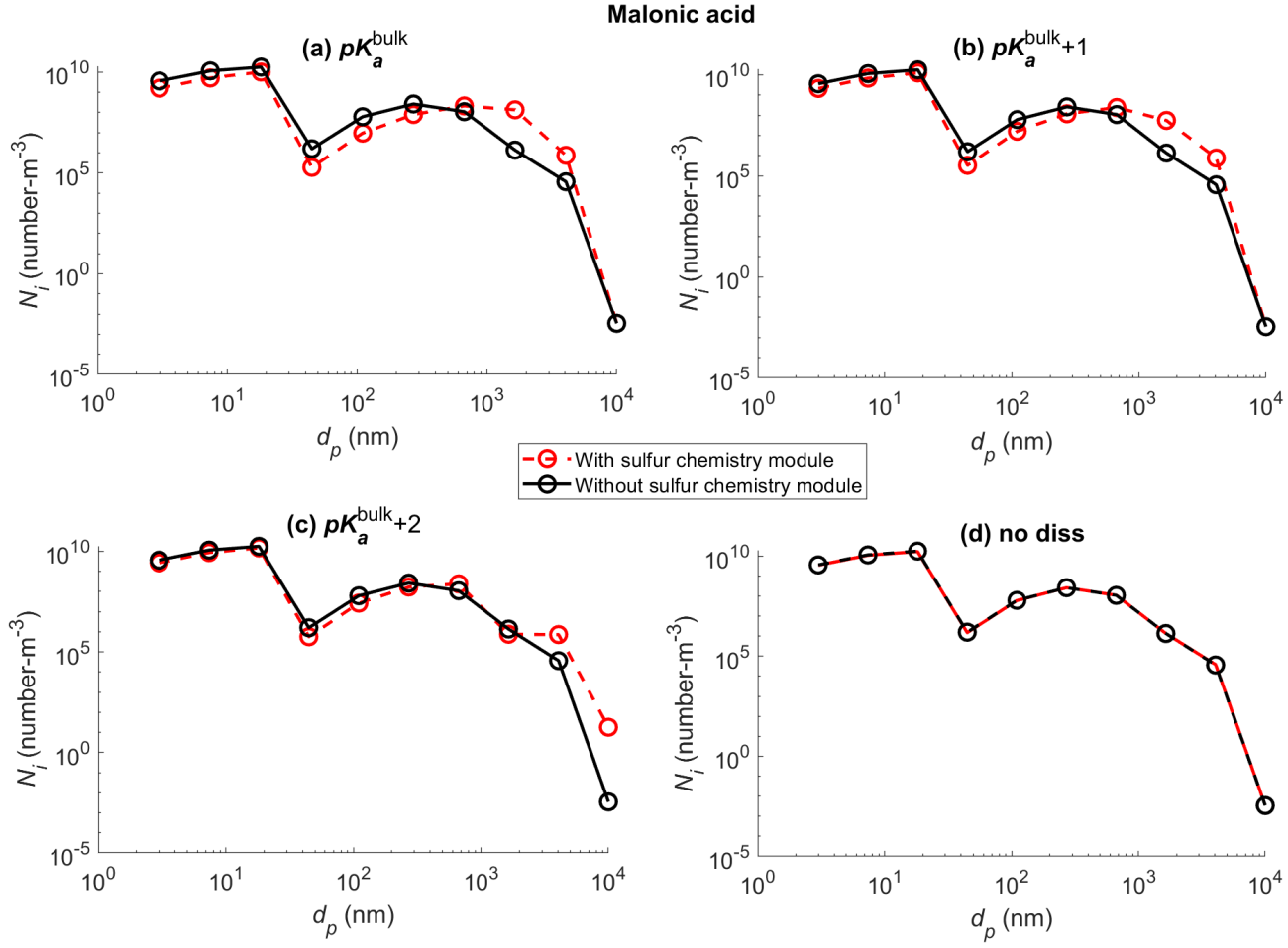

Figure A2. Particle size distribution represented by the number concentration (N_i) as a function od particle diameter (d_p) after 1 hour simulation time with and without activating the sulfur chemistry module for OA = malonic acid with χ_{OA} 0.8, considering the three representations of organic dissociation with apparent pK_a of (a) pK_a^{bulk}, (b) pK_a^{bulk}+1, (c) pK_a^{bulk}+2. Sub-figure (d) shows the same simulations without accounting for organic dissociation (no diss).

https://doi.org/10.5194/egusphere-2023-438
Preprint. Discussion started: 28 March 2023

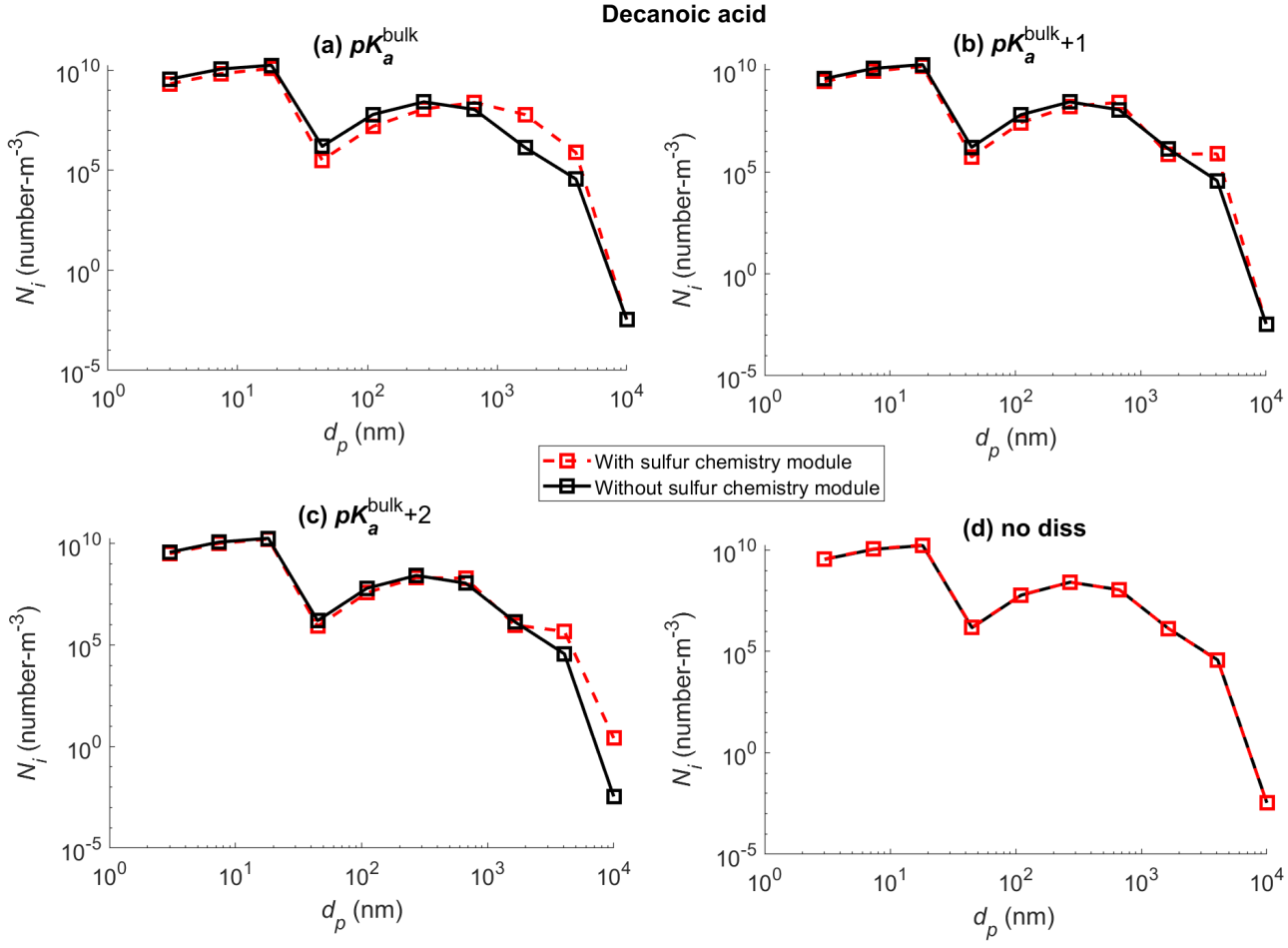

Figure A3. Particle size distribution represented by the number concentration (N_i) as a function od particle diameter (d_p) after 1 hour simulation time with and without activating the sulfur chemistry module for OA = decanoic acid with χ_{OA} 0.8, considering the three representations of organic dissociation with apparent pK_a of (a) pK_a^{bulk}, (b) pK_a^{bulk}+1, (c) pK_a^{bulk}+2. Sub-figure (d) shows the same simulations without accounting for organic dissociation (no diss).

https://doi.org/10.5194/egusphere-2023-438
Preprint. Discussion started: 28 March 2023

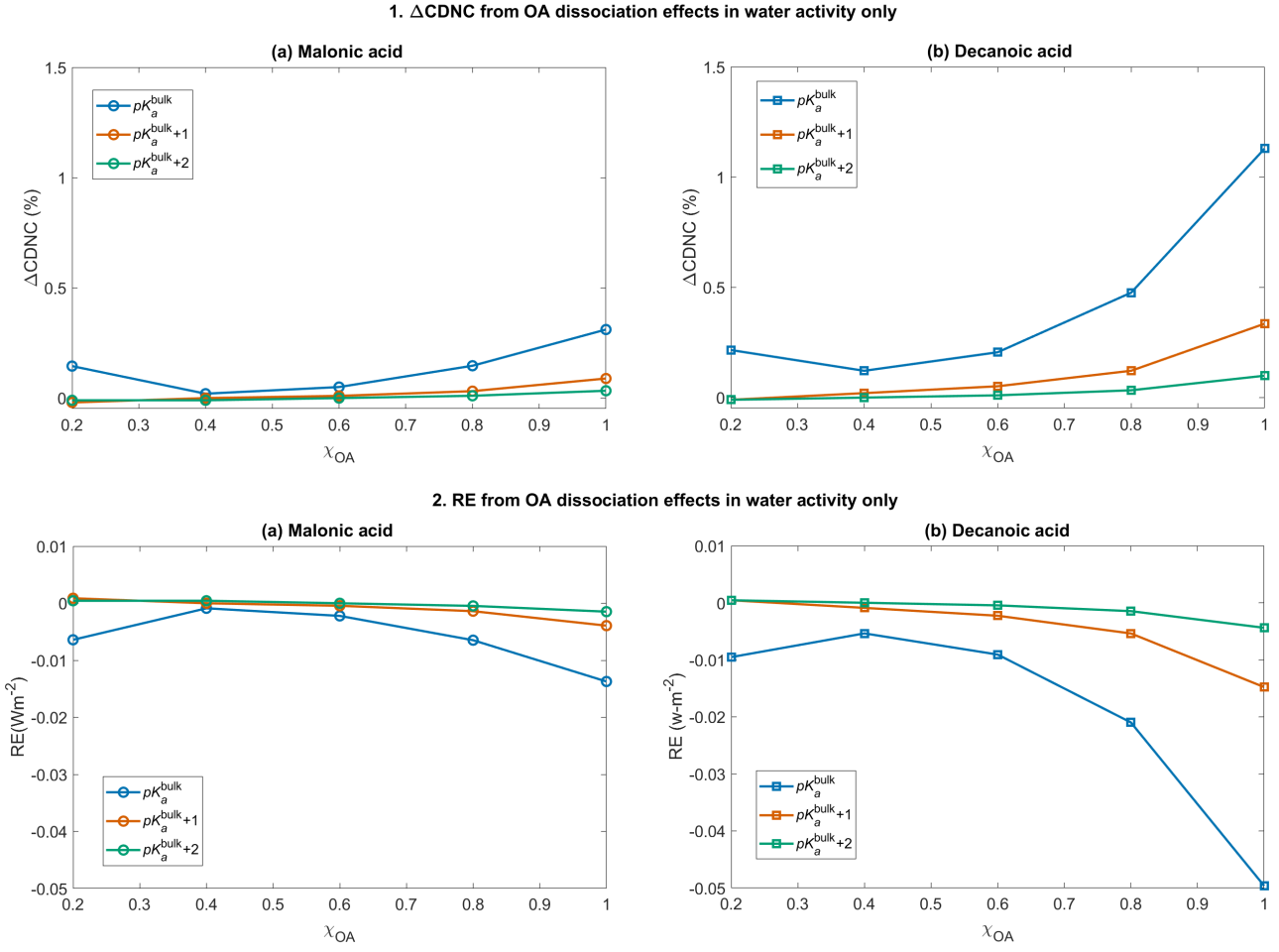

Figure A4. Organic dissociation effects in 1) cloud droplet number concentration ($\Delta CDNC$, calculated using equation 10) and 2) the resulting short-wave radiative effect (RE, calculated using equation 12) with respect to 'no diss',for varying initial organic mass fractions (χ_{OA}) assuming bulk organic dissociation (pK_a^{bulk}, blue) and surface modulated organic dissociation (pK_a^{bulk}+1, orange and pK_a^{bulk}+2, green), through changes in van't Hoff factor and water activity only. The sulfur chemistry module has not been activated in these simulations. (a) OA = malonic acid and (b) OA = decanoic acid.

Author contributions. GS did the model implementations and performed the calculations with contributions from MZ. GS and NLP analyzed the results and wrote the paper. NLP conceived, planned, supervised and secured funding for the project. All authors approved the final text.

Competing interests. The authors declare that there is no conflict of interest.

https://doi.org/10.5194/egusphere-2023-438
Preprint. Discussion started: 28 March 2023

Acknowledgements. The authors warmly thank Kunal Ghosh and Harri Kokkola for valuable support on HAMBOX. This project has received funding from the European Research Council (ERC) under the European Union's Horizon 2020 research and innovation program, project SURFACE (grant agreement no. 717022). The authors also gratefully acknowledge the financial contribution from the Academy of Finland, including grant nos. 308238, 314175, and 335649.

https://doi.org/10.5194/egusphere-2023-438
Preprint. Discussion started: 28 March 2023

References

Abdul-Razzak, H.: A parameterization of aerosol activation 3. Sectional representation, Journal of Geophysical Research, 107, https://doi.org/10.1029/2001jd000483, 2002.

Abdul-Razzak, H. and Ghan, S. J.: A parameterization of aerosol activation 3. Sectional representation, Journal of Geophysical Research: Atmospheres, 107, AAC–1, 2002.

Abdul-Razzak, H., Ghan, S. J., and Rivera-Carpio, C.: A parameterization of aerosol activation: 1. Single aerosol type, Journal of Geophysical Research: Atmospheres, 103, 6123–6131, https://doi.org/10.1029/97jd03735, 1998.

Äijälä, M., Daellenbach, K. R., Canonaco, F., Heikkinen, L., Junninen, H., Petäjä, T., Kulmala, M., Prévôt, A. S., and Ehn, M.: Constructing a data-driven receptor model for organic and inorganic aerosol–a synthesis analysis of eight mass<? xmltex\break?> spectrometric data sets from a boreal forest site, Atmospheric Chemistry and Physics, 19, 3645–3672, 2019.

Andreae, M. O. and Crutzen, P. J.: Atmospheric aerosols: Biogeochemical sources and role in atmospheric chemistry, Science, 276, 1052–1058, 1997.

Angle, K. J., Crocker, D. R., Simpson, R. M., Mayer, K. J., Garofalo, L. A., Moore, A. N., Mora Garcia, S. L., Or, V. W., Srinivasan, S., Farhan, M., et al.: Acidity across the interface from the ocean surface to sea spray aerosol, Proceedings of the National Academy of Sciences, 118, e2018397 118, 2021.

Ault, A. P.: Aerosol Acidity: Novel measurements and implications for atmospheric chemistry, Accounts of Chemical Research, 53, 1703–1714, 2020.

Battaglia Jr, M. A., Balasus, N., Ball, K., Caicedo, V., Delgado, R., Carlton, A. G., and Hennigan, C. J.: Urban aerosol chemistry at a land–water transition site during summer–Part 2: Aerosol pH and liquid water content, Atmospheric Chemistry and Physics, 21, 18 271–18 281, 2021.

Bzdek, B. R., Reid, J. P., Malila, J., and Prisle, N. L.: The surface tension of surfactant-containing, finite volume droplets, Proceedings of the National Academy of Sciences, 117, 8335–8343, 2020.

Drexler, C., Elias, H., Fecher, B., and Wannowius, K.: Kinetic investigation of sulfur (IV) oxidation by peroxo compounds R-OOH in aqueous solution, Fresenius' journal of analytical chemistry, 340, 605–615, 1991.

Dusek, U., Frank, G., Hildebrandt, L., Curtius, J., Schneider, J., Walter, S., Chand, D., Drewnick, F., Hings, S., Jung, D., et al.: Size matters more than chemistry for cloud-nucleating ability of aerosol particles, Science, 312, 1375–1378, 2006.

Feichter, J., Kjellström, E., Rodhe, H., Dentener, F., Lelieveldi, J., and Roelofs, G.-J.: Simulation of the tropospheric sulfur cycle in a global climate model, Atmospheric Environment, 30, 1693–1707, 1996a.

Feichter, J., Kjellström, E., Rodhe, H., Dentener, F., Lelieveldi, J., and Roelofs, G.-J.: Simulation of the tropospheric sulfur cycle in a global climate model, Atmospheric Environment, 30, 1693–1707, https://doi.org/https://doi.org/10.1016/1352-2310(95)00394-0, 1996b.

Franco, B., Blumenstock, T., Cho, C., Clarisse, L., Clerbaux, C., Coheur, P.-F., De Mazière, M., De Smedt, I., Dorn, H.-P., Emmerichs, T., et al.: Ubiquitous atmospheric production of organic acids mediated by cloud droplets, Nature, 593, 233–237, 2021.

Freedman, M. A., Ott, E.-J. E., and Marak, K. E.: Role of pH in aerosol processes and measurement challenges, The Journal of Physical Chemistry A, 123, 1275–1284, 2018.

Gérard, V., Noziere, B., Baduel, C., Fine, L., Frossard, A. A., and Cohen, R. C.: Anionic, cationic, and nonionic surfactants in atmospheric aerosols from the baltic coast at asko¨, sweden: Implications for cloud droplet activation, Environmental Science & Technology, 50, 2974–2982, 2016.

https://doi.org/10.5194/egusphere-2023-438
Preprint. Discussion started: 28 March 2023

Gérard, V., Noziere, B., Fine, L., Ferronato, C., Singh, D. K., Frossard, A. A., Cohen, R. C., Asmi, E., Lihavainen, H., Kiveka¨s, N., et al.: Concentrations and adsorption isotherms for amphiphilic surfactants in PM1 aerosols from different regions of Europe, Environmental science & technology, 53, 12 379–12 388, 2019.

Hennigan, C., Izumi, J., Sullivan, A., Weber, R., and Nenes, A.: A critical evaluation of proxy methods used to estimate the acidity of atmospheric particles, Atmospheric Chemistry and Physics, 15, 2775–2790, 2015.

Hudson, J. G. and Da, X.: Volatility and size of cloud condensation nuclei, Journal of Geophysical Research: Atmospheres, 101, 4435–4442, 1996.

Huebert, B., Bertram, T., Kline, J., Howell, S., Eatough, D., and Blomquist, B.: Measurements of organic and elemental carbon in Asian outflow during ACE-Asia from the NSF/NCAR C-130, Journal of Geophysical Research: Atmospheres, 109, 2004.

IPCC: The physical science basis, Contribution of working group I to the fifth assessment report of the intergovernmental panel on climate change, 1535, 2013, 2013.

IPCC, C. C. et al.: The physical science basis. Contribution of working group I to the fourth assessment report of the Intergovernmental Panel on Climate Change, Cambridge University Press, Cambridge, United Kingdom and New York, NY, USA, 996, 113–119, 2007.

Jacobson, M. Z.: Fundamentals of Atmospheric Modeling, Cambridge University Press, Cambridge, 2 edn., https://doi.org/DOI: 10.1017/CBO9781139165389, 2005.

Kanakidou, M., Seinfeld, J., Pandis, S., Barnes, I., Dentener, F. J., Facchini, M. C., Van Dingenen, R., Ervens, B., Nenes, A., Nielsen, C., et al.: Organic aerosol and global climate modelling: a review, Atmospheric Chemistry and Physics, 5, 1053–1123, 2005.

Kokkola, H., Kühn, T., Laakso, A., Bergman, T., Lehtinen, K. E., Mielonen, T., Arola, A., Stadtler, S., Korhonen, H., Ferrachat, S., et al.: SALSA2. 0: The sectional aerosol module of the aerosol–chemistry–climate model ECHAM6. 3.0-HAM2. 3-MOZ1. 0, Geoscientific model development, 11, 3833–3863, 2018.

Krofliˆc, A., Frka, S., Simmel, M., Wex, H., and Grgic´, I.: Size-resolved surface-active substances of atmospheric aerosol: Reconsideration of the impact on cloud droplet formation, Environmental science & technology, 52, 9179–9187, 2018.

Lee, L., Pringle, K., Reddington, C., Mann, G., Stier, P., Spracklen, D., Pierce, J., and Carslaw, K.: The magnitude and causes of uncertainty in global model simulations of cloud condensation nuclei, Atmospheric Chemistry and Physics, 13, 8879–8914, 2013.

Legg, S.: IPCC, 2021: Climate change 2021-the physical science basis, Interaction, 49, 44–45, 2021.

Li, J., Zhu, C., Chen, H., Fu, H., Xiao, H., Wang, X., Herrmann, H., and Chen, J.: A more important role for the ozone-S (IV) oxidation pathway due to decreasing acidity in clouds, Journal of Geophysical Research: Atmospheres, 125, e2020JD033 220, 2020.

Li, M., Su, H., Zheng, G., Kuhn, U., Kim, N., Li, G., Ma, N., Po¨schl, U., and Cheng, Y.: Aerosol pH and Ion Activities of HSO4–and SO42–in Supersaturated Single Droplets, Environmental Science & Technology, 56, 12 863–12 872, 2022.

Lin, J. J., Malila, J., and Prisle, N. L.: Cloud droplet activation of organic–salt mixtures predicted from two model treatments of the droplet surface, Environmental Science: Processes & Impacts, 20, 1611–1629, 2018.

Lin, J. J., Kristensen, T. B., Calderón, S. M., Malila, J., and Prisle, N. L.: Effects of surface tension time-evolution for CCN activation of a complex organic surfactant, Environmental Science: Processes & Impacts, 22, 271–284, 2020.

Liu, T., Clegg, S. L., and Abbatt, J. P.: Fast oxidation of sulfur dioxide by hydrogen peroxide in deliquesced aerosol particles, Proceedings of the National Academy of Sciences, 117, 1354–1359, 2020.

Maaß, F., Elias, H., and Wannowius, K. J.: Kinetics of the oxidation of hydrogen sulfite by hydrogen peroxide in aqueous solution:: ionic strength effects and temperature dependence, Atmospheric Environment, 33, 4413–4419, 1999.

https://doi.org/10.5194/egusphere-2023-438
Preprint. Discussion started: 28 March 2023

Malila, J. and Prisle, N.: A monolayer partitioning scheme for droplets of surfactant solutions, Journal of advances in modeling earth systems, 10, 3233–3251, 2018.

Martell, A. E. and Smith, R. M.: Critical stability constants, vol. 1, Springer, 1974.

McArdle, J. V. and Hoffmann, M. R.: Kinetics and mechanism of the oxidation of aquated sulfur dioxide by hydrogen peroxide at low pH, The Journal of Physical Chemistry, 87, 5425–5429, 1983.

McFiggans, G., Artaxo, P., Baltensperger, U., Coe, H., Facchini, M. C., Feingold, G., Fuzzi, S., Gysel, M., Laaksonen, A., Lohmann, U., et al.: The effect of physical and chemical aerosol properties on warm cloud droplet activation, Atmospheric Chemistry and Physics, 6, 2593–2649, 2006.

Murphy, D., Cziczo, D., Froyd, K., Hudson, P., Matthew, B., Middlebrook, A., Peltier, R., Sullivan, A., Thomson, D., and Weber, R.: Single-particle mass spectrometry of tropospheric aerosol particles, Journal of Geophysical Research: Atmospheres, 111, 2006.

Narukawa, M., Kawamura, K., Li, S.-M., and Bottenheim, J.: Dicarboxylic acids in the Arctic aerosols and snowpacks collected during ALERT 2000, Atmospheric Environment, 36, 2491–2499, 2002.

Nozière, B., Gérard, V., Baduel, C., and Ferronato, C.: Extraction and characterization of surfactants from atmospheric aerosols, JoVE (Journal of Visualized Experiments), p. e55622, 2017.

O'Dowd, C. D., Facchini, M. C., Cavalli, F., Ceburnis, D., Mircea, M., Decesari, S., Fuzzi, S., Yoon, Y. J., and Putaud, J.-P.: Biogenically driven organic contribution to marine aerosol, Nature, 431, 676–680, 2004.

Öhrwall, G., Prisle, N. L., Ottosson, N., Werner, J., Ekholm, V., Walz, M.-M., and Bjo¨rneholm, O.: Acid–base speciation of carboxylate ions in the surface region of aqueous solutions in the presence of ammonium and aminium ions, The Journal of Physical Chemistry B, 119, 4033–4040, 2015.

Peng, X., Vasilakos, P., Nenes, A., Shi, G., Qian, Y., Shi, X., Xiao, Z., Chen, K., Feng, Y., and Russell, A. G.: Detailed analysis of estimated pH, activity coefficients, and ion concentrations between the three aerosol thermodynamic models, Environmental Science & Technology, 53, 8903–8913, 2019.

Petters, S. S. and Petters, M. D.: Surfactant effect on cloud condensation nuclei for two-component internally mixed aerosols, Journal of Geophysical Research: Atmospheres, 121, 1878–1895, 2016.

Prisle, N., Dal Maso, M., and Kokkola, H.: A simple representation of surface active organic aerosol in cloud droplet formation, Atmospheric Chemistry and Physics, 11, 4073–4083, 2011.

Prisle, N., Asmi, A., Topping, D., Partanen, A.-I., Romakkaniemi, S., Dal Maso, M., Kulmala, M., Laaksonen, A., Lehtinen, K., McFiggans, G., et al.: Surfactant effects in global simulations of cloud droplet activation, Geophysical research letters, 39, 2012a.

Prisle, N., Ottosson, N., Öhrwall, G., Söderström, J., Dal Maso, M., and Björneholm, O.: Surface/bulk partitioning and acid/base speciation of aqueous decanoate: direct observations and atmospheric implications, Atmospheric Chemistry and Physics, 12, 12 227–12 242, 2012b.

Prisle, N. L.: A predictive thermodynamic framework of cloud droplet activation for chemically unresolved aerosol mixtures, including surface tension, non-ideality, and bulk–surface partitioning, Atmospheric Chemistry and Physics, 21, 16 387–16 411, 2021.

Prisle, N. L., Raatikainen, T., Laaksonen, A., and Bilde, M.: Surfactants in cloud droplet activation: mixed organic-inorganic particles, Atmospheric Chemistry and Physics, 10, 5663–5683, 2010.

Putaud, J.-P., Raes, F., Van Dingenen, R., Brüggemann, E., Facchini, M.-C., Decesari, S., Fuzzi, S., Gehrig, R., Hüglin, C., Laj, P., et al.: A European aerosol phenomenology—2: chemical characteristics of particulate matter at kerbside, urban, rural and background sites in Europe, Atmospheric environment, 38, 2579–2595, 2004.

https://doi.org/10.5194/egusphere-2023-438
Preprint. Discussion started: 28 March 2023

Putaud, J.-P., Van Dingenen, R., Alastuey, A., Bauer, H., Birmili, W., Cyrys, J., Flentje, H., Fuzzi, S., Gehrig, R., Hansson, H.-C., et al.: A European aerosol phenomenology–3: Physical and chemical characteristics of particulate matter from 60 rural, urban, and kerbside sites across Europe, Atmospheric Environment, 44, 1308–1320, 2010.

Pye, H. O., Nenes, A., Alexander, B., Ault, A. P., Barth, M. C., Clegg, S. L., Collett Jr, J. L., Fahey, K. M., Hennigan, C. J., Herrmann, H., et al.: The acidity of atmospheric particles and clouds, Atmospheric chemistry and physics, 20, 4809–4888, 2020.

Roberts, G. C., Andreae, M. O., Zhou, J., and Artaxo, P.: Cloud condensation nuclei in the Amazon Basin:"Marine" conditions over a continent?, Geophysical research letters, 28, 2807–2810, 2001.

Ruan, X., Zhao, C., Zaveri, R. A., He, P., Wang, X., Shao, J., and Geng, L.: Simulations of aerosol pH in China using WRF-Chem (v4. 0): sensitivities of aerosol pH and its temporal variations during haze episodes, Geoscientific Model Development, 15, 6143–6164, 2022.

Saxena, P. and Hildemann, L. M.: Water-soluble organics in atmospheric particles: A critical review of the literature and application of thermodynamics to identify candidate compounds, Journal of atmospheric chemistry, 24, 57–109, 1996.

Seinfeld, J. H., Bretherton, C., Carslaw, K. S., Coe, H., DeMott, P. J., Dunlea, E. J., Feingold, G., Ghan, S., Guenther, A. B., Kahn, R., et al.: Improving our fundamental understanding of the role of aerosol- cloud interactions in the climate system, Proceedings of the National Academy of Sciences, 113, 5781–5790, 2016.

Stahl, P. H. and Wermuth, C. G.: Handbook of pharmaceutical salts: properties, selection and use, Chem. Int, 24, 21, 2002.

Svenningsson, B., Rissler, J., Swietlicki, E., Mircea, M., Bilde, M., Facchini, M., Decesari, S., Fuzzi, S., Zhou, J., Mønster, J., et al.: Hygroscopic growth and critical supersaturations for mixed aerosol particles of inorganic and organic compounds of atmospheric relevance, Atmospheric Chemistry and Physics, 6, 1937–1952, 2006.

Tedetti, M., Kawamura, K., Charrière, B., Chevalier, N., and Sempéré, R.: Determination of low molecular weight dicarboxylic and ketocarboxylic acids in seawater samples, Analytical chemistry, 78, 6012–6018, 2006.

Tegen, I., Neubauer, D., Ferrachat, S., Siegenthaler-Le Drian, C., Bey, I., Schutgens, N., Stier, P., Watson-Parris, D., Stanelle, T., Schmidt, H., et al.: The global aerosol–climate model ECHAM6. 3–HAM2. 3–Part 1: Aerosol evaluation, Geoscientific Model Development, 12, 1643–1677, 2019.

Thompson, A.: Simulating the adiabatic ascent of atmospheric air parcels using the cloud chamber, Department of Meteorology, Penn State, pp. 121–123, 2007.

Tilgner, A., Bräuer, P., Wolke, R., and Herrmann, H.: Modelling multiphase chemistry in deliquescent aerosols and clouds using CAPRAM3. 0i, Journal of Atmospheric Chemistry, 70, 221–256, 2013.

Tilgner, A., Schaefer, T., Alexander, B., Barth, M., Collett Jr, J. L., Fahey, K. M., Nenes, A., Pye, H. O., Herrmann, H., and McNeill, V. F.: Acidity and the multiphase chemistry of atmospheric aqueous particles and clouds, Atmospheric Chemistry and Physics, 21, 13 483–13 536, 2021a.

Tilgner, A., Schaefer, T., Alexander, B., Barth, M., Collett Jr, J. L., Fahey, K. M., Nenes, A., Pye, H. O. T., Herrmann, H., and McNeill, V. F.: Acidity and the multiphase chemistry of atmospheric aqueous particles and clouds, Atmospheric Chemistry and Physics, 21, 13 483–13 536, https://doi.org/10.5194/acp-21-13483-2021, 2021b.

Vepsäläinen, S., Calderón, S. M., Malila, J., and Prisle, N. L.: Comparison of six approaches to predicting droplet activation of surface active aerosol–Part 1: moderately surface active organics, Atmospheric Chemistry and Physics, 22, 2669–2687, 2022.

Vepsäläinen, S., Calderón, S. M., and Prisle, N. L.: Comparison of six approaches to predicting droplet activation of surface active aerosol–Part 2: strong surfactants, EGUsphere, pp. 1–23, 2023.

https://doi.org/10.5194/egusphere-2023-438
Preprint. Discussion started: 28 March 2023

von Bismarck-Osten, C., Birmili, W., Ketzel, M., Massling, A., Petäjä, T., and Weber, S.: Characterization of parameters influencing the spatio-temporal variability of urban particle number size distributions in four European cities, Atmospheric environment, 77, 415–429, 2013.

Werner, J., Persson, I., Björneholm, O., Kawecki, D., Saak, C.-M., Walz, M.-M., Ekholm, V., Unger, I., Valtl, C., Caleman, C., et al.: Shifted equilibria of organic acids and bases in the aqueous surface region, Physical Chemistry Chemical Physics, 20, 23 281–23 293, 2018.